University Library

MINERVA ACCESS

A gateway to Melbourne's research publications

Minerva Access is the Institutional Repository of The University of Melbourne

Author/s:
Hood, AVS;Penman, DE;Lechte, MA;Wallace, MW;Giddings, JA;Planavsky, NJ

Title:
Neoproterozoic syn-glacial carbonate precipitation and implications for a snowball Earth

Date:
2022-03-01

Citation:
Hood, A. V. S., Penman, D. E., Lechte, M. A., Wallace, M. W., Giddings, J. A. & Planavsky, N. J. (2022). Neoproterozoic syn-glacial carbonate precipitation and implications for a snowball Earth. Geobiology, 20 (2), pp.175-193. https://doi.org/10.1111/gbi.12470.

Persistent Link:
https://hdl.handle.net/11343/298996

Check for updates

Neoproterozoic syn-glacial carbonate precipitation and implications for a snowball Earth

Ashleigh v.S. Hood*[1], Donald E. Penman[2], Maxwell A. Lechte[3], Malcolm W. Wallace[1], Jonathan A. Giddings[1], Noah J. Planavsky[2]

[1]School of Earth Sciences, University of Melbourne, Parkville, VIC 3010 Australia

[2]Department of Geology and Geophysics, Yale University, New Haven, CT 06511 USA

[3]Department of Earth and Planetary Sciences, McGill University, Montreal, Quebec H3A 0E8, Canada

*Corresponding author email: ashleigh.hood@unimelb.edu.au

Author Manuscript

Acknowledgements

The authors acknowledge the Adnyamathanha People, who are the traditional owners of the land where we undertook fieldwork. We would like to thank Warwick family of Holowilena South who have kindly allowed access to their property for research over many years. We also thank Brennan O'Connell for assistance during fieldwork; Rain Song for discussion; and Russell Drysdale for isotope work. We would like to thank the editor, Kurt Konhauser, as well as Linda Kah and two anonymous reviewers whose comments improved the manuscript. A.H. acknowledges funding from an ARC DECRA DE190100988; and M.W. and A.H were also supported by ARC DP210103715. NJP acknowledges funding from the NASA Alternative Earths Astrobiology Institute.

This is the author manuscript accepted for publication and has undergone full peer review but has not been through the copyediting, typesetting, pagination and proofreading process, which may lead to differences between this version and the Version of Record. Please cite this article as doi: 10.1111/GBI.12470

This article is protected by copyright. All rights reserved

DR. ASHLEIGH HOOD (Orcid ID : 0000-0002-1430-2371)

Article type : Original Article

Neoproterozoic syn-glacial carbonate precipitation and implications for a snowball Earth

Abstract

The Neoproterozoic "snowball Earth" hypothesis suggests that a runaway ice-albedo feedback led to two intense glaciations around 717–635 million years ago, and this global ice cover would have drastically impacted biogeochemical cycles. Testing the predictions of this hypothesis against the rock record is key to understanding Earth's surface evolution in the Neoproterozoic. A central tenet of the snowball Earth hypothesis is that extremely high atmospheric CO_2 levels—supplied by volcanic degassing over millions of years—would be required to overcome a strong ice-albedo feedback and trigger deglaciation. This requires severely diminished continental weathering (and associated CO_2 drawdown) during glaciation, and implies that carbonate minerals would not precipitate from syn-glacial seawater due to a lack of alkalinity influxes into ice-covered oceans. In this scenario, syn-glacial seawater chemistry should instead be dominated by chemical exchange with the oceanic crust and volcanic systems, developing low pH and low Mg/Ca ratios. However, sedimentary rocks deposited during the Sturtian glaciation from the Adelaide Fold Belt—and contemporaneous successions globally—show evidence for syn-sedimentary dolomite precipitation in glaciomarine environments. The dolomitic composition of these syn-glacial sediments and post-glacial 'cap carbonates' implies that carbonate precipitation and Mg cycling must have remained active during the ~50 million-year Sturtian glaciation. These syn-glacial carbonates highlight a gap in our understanding of continental weathering—and therefore the carbon cycle—during snowball Earth. In light of these observations, a Precambrian global biogeochemical model (PreCOSCIOUS) was modified to explore scenarios of syn-glacial chemical weathering, ocean chemistry, and Sturtian carbonate mineralogy. Modelling results suggest that a small degree of chemical weathering during

This article is protected by copyright. All rights reserved

Author Manuscript

glaciation would have been capable of maintaining high seawater Mg/Ca ratios and carbonate precipitation throughout the Sturtian glaciation. This is consistent with a severe ice age during the Sturtian, but challenges predictions of biogeochemical cycling during the endmember 'hard snowball' models. A small degree of continental weathering might also help explain the extreme duration of the Sturtian glaciation, which appears to have been the longest ice age in Earth history.

1. Introduction

The weathering of silicate minerals—and the subsequent deposition of carbonate minerals—is one of the key sinks of atmospheric CO_2, and the temperature dependence of this process is believed to stabilise global climate on geological time scales (Walker, Hays & Kasting, 1981). The discovery of extensive Neoproterozoic glacial deposits on multiple continents, and their apparent deposition at sea level at low palaeo-latitudes, led early researchers to suggest one or more global ice age occurred during this time (e.g. Harland, 1964), representing severe climate perturbations. According to global climate models, the presence of low latitude ice sheets would be expected to lead to a catastrophic runaway ice age due to the positive feedback of the albedo effect (Budyko 1969), with the accumulation of atmospheric CO_2 due to the near-complete shutdown of continental silicate weathering a possible avenue to overcome this phenomenon (Walker et al. 1981). As such, in effort to reconcile geological evidence for global glaciation with climate modelling, the "snowball Earth" hypothesis was developed (Kirschvink, 1992; Hoffman, Kaufman, Halverson & Schrag 1998; Hoffman et al., 2017). In this hypothesis, widespread ('snowball') ice coverage would have led to the near-total shutdown of silicate weathering, resulting in the accumulation of atmospheric CO_2, and rapid deglaciation after a threshold pCO_2 was reached after millions of years.

Our understanding of this Neoproterozoic climate change is heavily influenced by the interpretation of low-latitude carbonate successions that bracket the glacial deposits (Harland, 1964; Hoffman et al., 1998). The overlying, enigmatic 'cap carbonate' units—commonly composed of dolomite—have light carbon isotopic signatures that have been suggested to represent a shutdown in biological activity and a decoupling of the marine and atmospheric carbon cycles due to oceanic ice coverage (Hoffman et al., 1998). In the most extreme model scenarios of the 'Snowball Earth' hypothesis, the near-total cessation of continental weathering processes would have starved the oceans of continentally sourced solutes (i.e., via

This article is protected by copyright. All rights reserved

Author Manuscript

riverine input), resulting in syn-glacial seawater chemistry dominated by hydrothermal inputs (e.g. Hoffman et al., 1998). This has been speculated to have led to unusual seawater chemistry, characterised by low pH conditions whereby high dissolved CO_2 would have resulted in widespread carbonate dissolution (Hoffman et al., 1998; Le Hir, Goddéris, Donnadieu & Ramstein, 2008) and low Mg/Ca ratios (due to the removal or exchange of seawater Mg^{2+} with crustal Ca^{2+} during seafloor alteration; Coogan and Gillis, 2018; Hardie, 1996; Hoffman et al., 1998).

Contrary to this prediction, it has been demonstrated that carbonate deposits do occur in many Neoproterozoic glacial successions globally, including those in Australia (Crossing and Gostin, 1994; Preiss, Gostin, McKirdy, Ashley, Williams & Schmidt, 2011; Le Heron, Busfield & Collins, 2014; Lechte and Wallace, 2015), Brazil (Pedrosa-Soares et al., 2011), Canada (Macdonald et al., 2018), USA (Lechte, Wallace, Hood & Planavsky, 2018), Scotland (Fairchild et al., 2018), Namibia (Hoffman et al., 2021), China (Yu et al., 2017) and Svalbard (Halverson, 2011; Mackey et al, 2020). These glacial carbonates–often composed of dolomite–have been typically considered to be detrital: i.e., sourced from the subglacial erosion of older, pre-glacial carbonate units (Fairchild and Hambrey, 1984; Fairchild, Hambrey, Spiro & Jefferson, 1989; Crossing and Gostin, 1994). A detrital origin for the glacial-associated carbonate (dolomite) would be consistent with several previously held assumptions about carbonates: (1) dolomite does not precipitate from modern 'normal' seawater ("the dolomite problem" e.g. Land, 1998); (2) marine carbonate does not readily precipitate from cold seawater; and (3) carbonate would not precipitate in postulated acidic 'snowball Earth' oceans (Hoffman et al., 1998).

However, with our present state of knowledge, these assumptions about carbonate precipitation have become less definitive. Firstly, it is recognised that marine dolomite precipitation was widespread in Neoproterozoic oceans (e.g. Tucker, 1982; Hood and Wallace, 2012; 2018; Hu et al., 2020; Cantine et al., 2020). Secondly, cool-water carbonates (though often skeletal) are now understood to form an important component of Phanerozoic and modern carbonate systems including glaciated margins (James, 1997; Rao, Goodwin & Gibson, 1998). Therefore, a re-evaluation of the origin of Neoproterozoic syn-glacial carbonates is required. The origin of these carbonate lithologies links directly to our understanding of carbon cycling during the Neoproterozoic, with important implications for the effects of severe climate change on Earth's surface environments.

This article is protected by copyright. All rights reserved

Author Manuscript

Although recent studies have offered valuable insights into the nature of key biogeochemical cycles during snowball Earth (e.g. Hoffman et al. 2017; Lechte et al. 2019; Mackey, Jost, Creveling & Bergmann 2020), significant gaps in our understanding of the impact of global glaciation remain. The sedimentological expression of carbonate rocks deposited during the Neoproterozoic Sturtian glaciation (ca. 717–660 Ma: Rooney, Strauss, Brandon & Macdonald, 2015) can help resolve syn-glacial ocean conditions. In order to test key predictions of the snowball Earth hypothesis against the rock record, we present a detailed study on a well-preserved, dolomite-rich succession within glacial deposits of the Yudnamutana Subgroup (South Australia; Preiss, 1987; Preiss et al., 2011)(Fig. 1). These dolomite units show sedimentological and geochemical evidence for precipitation from seawater during the Sturtian glaciation. We evaluate the significance of these deposits in light of the extent of similar sedimentological evidence presented in the published literature. Based on these geological observations from Australia, in conjunction with evidence from carbonates within Neoproterozoic glacial successions elsewhere, scenarios of Sturtian glaciation consistent with syn-glacial dolomite precipitation are explored with the geochemical model PreCOSCIOUS (Penman and Rooney, 2019).

2. Geological background

Late Tonian stratigraphy of the Flinders Ranges is represented by the Burra Group, which is unconformably overlain by early Cryogenian glacial sediments of the Yudnamutana Subgroup (Preiss, 1987). The Tonian Burra Group consists of a thick succession of shale, siltstone, dolostone and sandstone, including characteristic white intraclastic magnesite lithologies of the Skillogalee Dolomite (Preiss, 1987; Frank and Fielding, 2003). A U-Pb zircon date for the upper stratigraphy in the Skillogalee Dolomite of 792 ± 6 Ma (Preiss, Drexel and Reid, 2009) broadly constrains the age of the preserved Burra Group and provides a maximum age for the Sturtian glaciation in South Australia.

The Sturtian glaciation in the Flinders Ranges is encompassed by the Yudnamutana Subgroup (Fig. 1a; Preiss, 1987; Preiss et al., 2011). The age of the Sturtian strata in this succession is poorly constrained. A U-Pb zircon date from the uppermost Yudnamutana Subgroup, near Copley, South Australia, of 663.03 ± 0.11 Ma constrains the timing of the end of the Sturtian glaciation (Cox et al., 2018). The onset of the Sturtian glaciation is not constrained geochronologically in the Adelaide Fold Belt, but is generally thought to have

This article is protected by copyright. All rights reserved

Author Manuscript

begun globally ca. 717 Ma based on the geochronology of several correlative Sturtian glacial successions (Rooney et al., 2015). The Sturtian glacial succession of the Yudnamutana Subgroup is overlain by a Sturtian 'cap carbonate', commonly composed of dolomite and reaching up to tens of metres in thickness (e.g. Giddings and Wallace, 2009a). Sedimentary rocks of the Yudnamutana Subgroup in the Flinders Ranges have generally experienced low- to mid-greenschist facies metamorphism (Preiss, 1987).

At Holowilena South in the Baratta Trough, the stratigraphy of the Yudnamutana Subgroup consists of the Pualco Tillite, Holowilena Ironstone and Wilyerpa Formation (which includes the lower Warcowie Dolomite Member) (Preiss, 1987; Preiss et al., 2011) (Fig 2-3). The lowermost formation of the Yudnamutana Subgroup comprises the Pualco Tillite which has been assigned to an early phase of Sturtian glaciation (Preiss, 1987). At Holowilena South, the Pualco Tillite is composed largely of massive, lonestone-bearing diamictite interbedded with shale; less abundant sandstone, dolomitic shale and dolomite beds, and represents an ice-proximal to ice-contact depositional environment (Lechte et al., 2019). The overlying ferruginous shales and resedimented diamictites of the Holowilena Ironstone (deposited in an ice-proximal setting: Lechte and Wallace, 2015; Lechte et al., 2019) are in turn disconformably overlain by a two-metre thick dolomite unit known as the Warcowie Dolomite Member (Preiss, 1987; Lechte and Wallace, 2015) (Fig. 3. 4a). This unit varies in thickness from decimeters to metres across lateral distance of ~2 kilometres at Holowilena South and lacks clear evidence of a proximal ice margin or ice grounding line in this locality (Lechte and Wallace, 2015). Nearby, at Mount Plantagenet, which is the type section of the basal Warcowie Dolomite Member, this unit contains a ~5 m thick, lower interval of dolomitic breccia, overlain by ~20 m of massive dolomite with rare pebbles, succeeded by conglomerate (Preiss, 1987). At Oraparinna, the upper Holowilena Ironstone is interbedded with yellow dolomite and dolomitic siltstones in transition into the Wilyerpa Fm., and these bedded and laminated carbonates are interpreted to have been deposited in an ice-distal glaciomarine environment (Lechte et al., 2019)(Fig. 4g-h).

At Holowilena South, the Pualco Tillite and Holowilena Ironstone are overlain by a <2 km succession of the Wilyerpa Formation, representing a younger interval of the Sturtian glaciation (Preiss, 1987). The Wilyerpa Formation features interbedded diamictite, sandstone and siltstone, including less common dolomite and dolomitic siltstone beds as well as dropstone intervals (which may occur in siltstones and dolomite-rich beds). An ice-distal

This article is protected by copyright. All rights reserved

Author Manuscript

environment is interpreted for the Wilyerpa Fm. at Holowilena South due to the abundance of fine-grained and laminated sediments (Lechte et al., 2019), though more broadly, the sequence shows multiple episodes of glacial advance and retreat (e.g. Young and Gostin, 1991; Le Heron et al., 2011).

At Oraparinna, near Panta Well, the base of the Yudnamutana Subgroup is missing, and the Holowilena Ironstone forms the first stratigraphic unit exposed adjacent to the Oraparinna diapiric breccia (Lechte et al., 2019)(Fig. 2-4). At this locality, the Holowilena Ironstone is ~120 m thick and has a gradational upper contact with the overlying Wilyerpa Formation. The lower Holowilena Ironstone contains ferruginous siltstone and minor diamictite, interpreted to be the product of deposition in an ice-proximal setting (Lechte et al., 2019).

In general, the Yudnamutana Subgroup includes abundant carbonate (generally dolomite) lithologies. Howchin (1918) was the first to document carbonate strata in the Neoproterozoic glacial deposits of South Australia, describing "thin, gritty and siliceous limestones" in the Sturt Tillite in the Adelaide region (Howchin, 1918, his p. 349). Carbonate is present—and sometimes a major constituent—in diamictite and bedded glacial facies associated with siltstones where it generally forms matrix material (Preiss, 1987; Preiss et al., 2011). There have been limited sedimentological and stable isotope studies of the carbonates within these glacial successions to date, (Crossing and Gostin, 1994; Walter, Veevers, Calver, Gorjan & Hill, 2000; McKirdy et al., 2001; Le Heron, Cox, Trundley & Collins, 2011; Le Heron et al., 2014; Lechte and Wallace, 2015; summary in Preiss et al., 2011).

3. Geological and geochemical methods

Stratigraphic sections were measured with a Jacob's Staff at Holowilena South and Oraparinna, Adelaide Fold Belt, South Australia. Samples were collected from carbonate-bearing lithologies identified in the field for petrographic work and stable isotope analysis along the measured sections at Holowilena South, and at Oraparinna in the Flinders Ranges, South Australia.

Polished petrographic thin sections (>20 samples) were made from selected Sturtian carbonate samples, focusing mainly on the Holowilena Ironstone, Warcowie Dolomite Member, and Wilyerpa Formation at Holowilena South. Thin sections of non-carbonate glacial facies at other localities were also studied for context. Thin sections were analysed

This article is protected by copyright. All rights reserved

Author Manuscript

using standard, cathodoluminescence and scanning electron microscopy (SEM) in the School of Geography, Earth and Atmospheric Sciences, University of Melbourne. Operating conditions for the cathodoluminoscope were an ~8 kV accelerating voltage and ~0.5 mA current. Scanning electron microscopy (SEM: Back Scatter Electron (BSE) imaging and semi-quantitative Energy Dispersive Spectroscopy (EDS)) was undertaken on coated samples on a JEOL JXA-8530F operated at 15 kV and a Philips FEI XL30 environmental scanning electron microscope equipped with an OXFORD INCA energy-dispersive X-ray spectrometer at the University of Melbourne. After representative petrographic analysis, cut hand samples were cleaned, and were drilled avoiding weathered rock, veins, non-carbonate inclusions and detrital clasts. The drilling targeted carbonate-rich beds and laminae. Powdered samples (~0.3g) were then homogenised in an agate mill to form a fine powder. Carbonate content was measured using standard acid digestion and volumetric carbonate analysis at the University of Melbourne (modified from Hülsemann, 1966).

Stable isotopes were measured on the same homogenised sample powders used for carbonate analysis on 0.7 - 0.9 mg subsamples using continuous-flow isotope-ratio mass spectrometry, on an Analytical Precision AP2003 in the School of Geography, Earth and Atmospheric Sciences, University of Melbourne. Samples were digested in 105% phosphoric acid at 70°C. Isotope ratios were determined on the evolved CO_2 gas and the results normalised to the Vienna Pee Dee Belemnite scale using the internal working standards of Carrara Marble (NEW1), which was cross-checked against the international standards NBS18 and NBS19. The data are presented in permil (‰) units as relative isotopic ratios for carbon ($\delta^{13}C$) and oxygen ($\delta^{18}O$), on the V-PDB scale. Analytical uncertainties are reported as ± 0.05 ‰ for carbon isotopes and ± 0.09 ‰ for oxygen isotopes (1 SD).

4. Sturtian syn-glacial carbonates of South Australia

4.1 Glacial Sedimentology and Stratigraphy

In order to gain insights into the nature and significance of Cryogenian syn-glacial carbonates, the well-preserved, carbonate-bearing glacial successions of the Flinders Ranges were studied at Holowilena South and Oraparinna. Broad facies and paleo-environmental interpretations for these sections are given in Lechte et al. (2019), and detailed in Section 2.

Author Manuscript

This article is protected by copyright. All rights reserved

Measured stratigraphic sections through the Yudnamutana Subgroup at Holowilena South reveal a glaciomarine succession with dolomite throughout the sequence (Fig. 3). Dolomitic lithologies are readily identifiable in outcrop due to their yellow, recessive, sometimes kluftkarren-bearing, weathering pattern. The uppermost Pualco Tillite, which underlies the Holowilena Ironstone, shows unstratified diamictites which may have dolomitic matrix and dolomite clasts. This unit has a relatively high abundance of dolomite overall in that both diamictite and bedded lithologies are yellow-recessive weathering and contain dolomite.

The Warcowie Dolomite is a distinctive ~2 m thick, laminated dolomite unit above the Holowilena Ironstone which grades from more clay-rich to more dolomite-rich towards the upper bed margin (Fig. 4a). Siltstones and diamictite units of the Wilyerpa Formation are often dolomitic (Fig. 4b–f), though large sections of the stratigraphy do not contain abundant carbonate. Dolomite beds of centimetres to decimetres in thickness may also be interbedded with siltstones or appear nodular, and dolomitic silt also forms the matrix of many diamictites. There are also abundant dolomite clasts in diamictite and dropstone shale lithologies within this unit. Some clasts show the characteristic white intraclastic dolomite and magnesite lithologies of the underlying Skillogalee Dolomite (Fig. 4g), while others are laminated yellow dolomite clasts that could have been derived from different units within the glacial sedimentary succession. There are also abundant lithic clasts and clasts of quartz, potassium feldspar, apatite, albite and minor calcite in all units at Holowilena South (Figs. 5-7).

The field relationships and petrography of the glacial dolomite lithologies reveal a range of sedimentary features. Dolomite beds of the Wilyerpa Formation and Holowilena Ironstone can be finely laminated, and in some layers show vaguely rhythmic alternation between dolomicrite and fine quartz sand (e.g. Fig 5a-c). Sand beds often resemble turbidites, with variable thickness and erosive bases, showing syn-sedimentary erosion and loading into carbonate layers (Fig 5 a, d, e). Rounded gravel and sand beds of lithic or mineral clasts (quartzite, carbonate and volcanic rock types are common) with a variable origin may occur within dolomitic matrix silts and dolomicrite layers within the Wilyerpa Fm (Fig 5. e, g, h). Diamictites of the Pualco Tillite (Fig. 5 j-k) and Wilyerpa Formation (Fig. 5l) have angular to rounded clasts of a variable lithologies, and feature abundant quartz grains in a dolomite-clay matrix. Overall, dolomite crystals form a minor to major proportion of the matrix material in

Author Manuscript

This article is protected by copyright. All rights reserved

a range of these facies and units. Dolomite matrix material is similar between samples, appearing as high-birefringent, anhedral-euhedral crystals in thin section (Fig. 5 c,f,I,kl).

The carbonate content of the Sturtian dolomitic lithologies from Holowilena South ranges between 19 % and 72 % (mean: 41 %; Table 1). Commonly, dolomite beds feature evidence of syn-sedimentary reworking including slump folding, erosion by quartz-sand turbidites and deformation by dropstones (Figs. 4c-d, 5). Gradation in the amount of dolomite present in beds is present, with many beds more dolomite-rich on their upper surface (though beds may be inversely graded with respect to dolomite or variable in their dolomite content along strike). At Holowilena South, the Warcowie Dolomite Member transitions from a clay-rich lithology (~35% carbonate) to more dolomite-rich (~65% carbonate) at its upper margin, over tens of centimetres to two metres in stratigraphic thickness. Dolomite is also present as matrix material in silt to fine sand beds through the Wilyerpa Formation. At Oraparinna, the upper Holowilena Ironstone contains yellow dolomitic siltstone units, where carbonate content ranges from 19% to 52% (mean: 36%), though some beds in the sequence are composed of non-calcareous yellow siltstones.

Petrographic analysis reveals that in all facies, dolomite is present as ~2–10 µm subhedral to euhedral (commonly anhedral to euhedral) matrix crystals which may embay siliciclastic detrital material (Fig. 6-7). Dolomite crystals appear bright- or dull-red luminescent under cathodoluminescence (Fig. 6a-b). Scanning electron microscopy (semi-quantitative EDS) on samples from all units at Holowilena South reveals fine-scale zonation in Fe content of the dolomite crystals and confirms a dolomite mineralogy with no geochemical or petrographic evidence of a detrital core (Figs. 6-7). Crystals sometimes show euhedral or subhedral growth banding defined by variation in iron content between cores and crystal rims (e.g. Fig. 6c-e, 7). Crystals may be simply or complexly zoned between Fe-rich (bright) and less Fe-rich (dark) zones, or may be either entirely Fe-rich or Fe-poor. These dolomite crystals show no abrasion, erosion or any related effects of transportation and weathering (Fig. 6c-e, 7).

4.2 Stable isotopes

Dolomite samples from Holowilena South and Oraparinna have carbon isotope ($\delta^{13}C$) values ranging between -5.1 to +1.5 ‰ (mean $\delta^{13}C$ = -1.4 ‰), with oxygen isotope ($\delta^{18}O$) values from -7.0 to +0.6 ‰ (mean $\delta^{18}O$ = -4.1 ‰) (Fig. 8; Table S1). Samples from the Wilyerpa Formation at Holowilena South (n = 22, mean $\delta^{18}O$ = -4.9 ‰) tend to be lighter in oxygen

This article is protected by copyright. All rights reserved

Author Manuscript

isotope composition than the Pualco Tillite (n = 3, mean $\delta^{18}O$ = -2.0 ‰). There is a weak trend of increasingly negative carbon isotopes values with stratigraphic height in the Wilyerpa Formation at Holowilena South (R^2= 0.41; Figure S1). Samples from the Holowilena Ironstone at Oraparinna are generally heavier in both $\delta^{13}C$ and $\delta^{18}O$ (mean $\delta^{13}C$ = 0.6 ‰, mean $\delta^{18}O$ = -1.4 ‰) compared to the broadly equivalent strata at Holowilena South (mean $\delta^{13}C$ = 0.3 ‰, mean $\delta^{18}O$ = -4.6 ‰). There are no clear correlations between $\delta^{13}C$ or $\delta^{18}O$ and glacial facies, lithology or carbonate concentrations in either location.

Previously reported stable isotope data from the late-Sturtian Wilyerpa Formation in the Frontier Blinman-2 drillcore shows dolomite diamictite samples with up to 20% carbonate and generally depleted $\delta^{13}C$ values of -5.3 to +2.0 ‰, with more positive values in the uppermost stratigraphy (McKirdy et al., 2001) (Fig. 8). Oxygen isotope values are also depleted, with an average of -9.8 ‰ and a range from -12.4 to -7.3 ‰ (McKirdy et al., 2001). Unlike most samples from this study, the carbonate samples of McKirdy et al. (2001) were sampled from diamictite facies of the Wilyerpa Formation. Therefore, it is unclear if these values result from detrital carbonate (i.e. diamictite clasts) or authigenic matrix carbonate. The early Sturtian Appila Tillite (equivalent to the Pualco Tillite, Preiss et al., 2011: Fig. 1a) has similar isotopic compositions to our new data from Holowilena South and Oraparinna (Crossing and Gostin, 1994). The average $\delta^{13}C$ value of the Appila Tillite matrix dolomite samples, including one nodule, was -0.80 ‰ (range: -2.26 to 1.20 ‰), with $\delta^{18}O$ values averaging -6.93 ‰ (range: -9.77 to -3.42 ‰)(Crossing and Gostin, 1994). In contrast, dolomite clasts show distinct and significantly more positive stable isotopic values (mean $\delta^{13}C$ = +4.39 ‰, range +2.27 to +5.27 ‰; mean $\delta^{18}O$ = +0.28 ‰, range -1.50 to +1.47 ‰)(Crossing and Gostin, 1994) (Fig. 8).

5. Geological Discussion

5.1 Syn-glacial dolomite precipitation in the Yudnamutana Subgroup

Dolomitic facies are abundant in the Yudnamutana Subgroup, and deciphering the origin of this dolomite enrichment—i.e., detrital resedimentation of pre-existing carbonate lithologies, authigenic marine precipitation or late-stage diagenesis—is crucial to extracting paleoenvironmental information from these deposits. Some dolomite is clearly detrital, and there are abundant clasts of dolomite, some of which appear to be derived from the underlying Burra Group stratigraphy (e.g. Fig. 4g; also see discussion in Crossing and Gostin, 1994). However, many of the dolomite units do not appear to have been transported. As such,

This article is protected by copyright. All rights reserved

Author Manuscript

for much of the carbonate-bearing stratigraphy including the dolomitic siltstones and other bedded dolomite, sedimentological evidence is more consistent with an authigenic, syn-sedimentary origin.

Substantial evidence of sedimentary reworking of the bedded dolomitic strata (e.g. deformation by dropstone emplacement, erosion by turbidite deposition, Fig. 4c, 5) does not support a late diagenetic origin, and instead suggests that dolomite precipitation occurred during or immediately following deposition. The observation of very finely laminated dolomicrite sediments, which preserve fine-scale sedimentary features, is also consistent with early dolomite precipitation. In all facies, the lack of evidence for detrital cores or mechanical grain reworking (e.g. abrasion) in the dolomite crystals argues against detrital transportation and suggests that the dolomite crystals precipitated in situ (Fig. 6-7). There is also no evidence of precursor carbonate mineral phases such as ikaite, which forms at low temperatures, though it is impossible to rule out that the possibility that a metastable precursor transformed to dolomite during diagenesis. The dolomite crystals are rhombic (trigonal), a different system to ikaite (monoclinic), and at a broader scale, there is no evidence of glendonites in the stratigraphy.

An early marine diagenetic origin for the dolomite is also supported by the combination of the anhedral to euhedral shape and fine crystal size of the dolomite. In contrast, though destructive dolomite replacement during higher temperature burial diagenesis is commonly euhedral, it is often coarsely crystalline. Some of the dolomitic beds, including the Warcowie Dolomite, are more dolomite-rich on their upper surface: this may suggest that dolomite precipitation occurred at the sediment–water interface and migrated downwards into the sediment. Alternatively, permeability and porosity of the sediment may have played a role in the extent of authigenic dolomite precipitation just below the sediment–water interface. Continued authigenic precipitation of dolomite in marine pore waters during ongoing sedimentation may explain the observation of some embayment of silicate grains by later crystal growth (e.g. Wallace et al., 2019). Cathodoluminescence and BSE image colour, brightness and zonation confirm a dolomitic mineralogy and indicate precipitation under anoxic fluid conditions (with dissolved Mn^{2+} and Fe^{2+}). This is consistent with ferruginous marine conditions during this time (e.g. marine iron (oxyhydr)oxide deposition; Lechte et al., 2019) but may also occur in diagenetic fluids.

This article is protected by copyright. All rights reserved

Author Manuscript

A syn-glacial origin for Sturtian dolomite precipitation from the Holowilena South succession, and regionally, is also supported by the carbon and oxygen isotope composition of these dolomite units. Glacial matrix dolomite samples have distinct carbon isotope compositions compared to dolomite clasts in diamictites (e.g. Crossing and Gostin, 1994), suggesting a different origin (Fig. 8). Based on their appearance in the field, many carbonate clasts within the Yudnamutana Subgroup diamictites appear to be derived from the underlying Burra Group stratigraphy (i.e. the distinctive intraclastic lithologies of the Skillogalee Dolomite; Preiss, 1987; Fig. 4g; also see discussion in Crossing and Gostin, 1994), which is dominated by heavier carbon and oxygen isotope values (Crossing and Gostin, 1994; Hill and Walter, 2000; Frank and Fielding, 2003) (Fig. 8). If the bedded dolomite lithologies of the Yudnamutana Subgroup were also the product of detrital reworking of the underlying carbonate lithologies, they should also be dominated by a positive $\delta^{13}C$ signal. Further, in addition to these bedded dolomite lithologies (which do not appear to be detrital in origin), detrital carbonate is isotopically distinct from the underlying carbonates suggesting reworking of a contemporaneous (syn-glacial) dolomite unit (Fig. 8, Crossing and Gostin, 1994).

The carbon isotopic signatures of the Yudnamutana Subgroup are instead more similar to typical non-glacial, deep-water carbonates from the overlying stratigraphy, including the post-glacial Sturtian cap carbonate (Tindelpina Shale Member); the Tapley Hill Formation and several dolomite marine hardgrounds, which show generally slightly depleted $\delta^{13}C$ values (McKirdy et al., 2001; Giddings and Wallace, 2009a, b; Preiss et al., 2011; Wallace, Hood, Fayle, Hordern, & O'Hare, 2019). The commonly negative $\delta^{13}C$ values of many of these deep-water dolomites—interpreted to be marine chemical sediments—and syn-glacial carbonates could be explained by a mix of carbon derived largely from marine dissolved inorganic carbon (DIC) and remineralized organic carbon sources, as interpreted more broadly for authigenic carbonates of the Proterozoic (e.g. Schrag, Higgins, Macdonald & Johnston, 2013; see discussion in Wallace et al., 2019).

Though speculative, the depleted $\delta^{18}O$ composition of Sturtian carbonates from South Australia may also be consistent with their syn-glacial precipitation. Equilibrium isotope fractionation during marine ice formation leads to isotopically light oxygen in residual seawater (O'Neil, 1968). Although the impact of global glaciation, including the extent of ice coverage, on the oxygen isotope composition of seawater is unclear (e.g. see discussion in

This article is protected by copyright. All rights reserved

Author Manuscript

Defliese, 2021), ice-water equilibrium fractionation could have led to negative $\delta^{18}O$ values in Cryogenian glaciated margins (Hoffman et al. 2017). However, it should be noted that oxygen isotopic composition of carbonates from this sequence are highly variable (Fig 6.) and could also be attributed to a range of other factors including post-depositional processes including diagenetic alteration.

5.2 Regional expression of dolomite lithologies in the Yudnamutana Subgroup

The sedimentology and geochemistry of the Yudnamutana Subgroup carbonate units described here—and the kilometre-scale stratigraphic thickness of these dolomite-bearing units—suggests that marine, syn-sedimentary dolomite precipitation was ongoing throughout the Sturtian glaciation in this Neoproterozoic basin. The variable glaciomarine facies associations of the carbonate units at Holowilena South, Oraparinna and elsewhere (Lechte et al., 2019) suggests that dolomite deposition occurred in a wide range of non-restricted, glaciomarine depositional environments. In order to consider the possible regional or global significance of the carbonate deposits described here, it is important to understand the spatiotemporal distribution of similar carbonate lithologies in other Sturtian successions.

Sturtian glacial units across many other localities in South Australia also contain dolomitic lithologies in a range of different glacial facies (Preiss, 1987; Crossing and Gostin, 1994; McKirdy et al., 2001; Preiss et al., 2011). In the Yudnamutana Trough of the Northern Flinders Ranges, the glaciomarine Bolla Bollana Tillite contains rare, laminated dolomite beds (Le Heron et al., 2014). In Weetootla Gorge, three intervals of dolomite are present and are described as “buff-coloured, delicately parallel laminated, mud-grade dolostones” (Le Heron et al., 2014). These carbonate units occur at the top of fining-up cycles, and are interpreted to represent precipitation during or following lobe abandonment in a submarine fan system, possibly under low depositional rates or ice-free interglacial conditions (Le Heron et al., 2014).

The Appila Tillite of the Emeroo Range and southern Flinders Ranges also contains abundant carbonate lithologies including a dolomite matrix for diamictite and shales (Crossing and Gostin, 1994). The Appila Tillite, equivalent to the Pualco Tillite, is interpreted to have been deposited in a shallow glaciomarine environment, featuring two sequences of glacial advance and retreat (Young and Gostin, 1990; Crossing and Gostin, 1994; Preiss et al., 2011). Crossing and Gostin (1994) demonstrate that the dolomitic matrix of the Appila Tillite

This article is protected by copyright. All rights reserved

Author Manuscript

diamictites have a distinct, more depleted (negative) $\delta^{13}C$ and $\delta^{18}O$ values compared to the dolomite clasts (Fig. 8). A high percentage of the iron in the Appila Tillite is bound in carbonate phases (25 to 96%; Canfield et al., 2008), which is consistent with Fe-dolomite precipitation at Holowilena and ferruginous syn-glacial marine conditions more broadly (Lechte et al., 2019).

Overall, the Yudnamutana Subgroup syn-glacial bedded dolomite units are similar in lithology, morphology and carbon isotope composition to dolomitic deep-water sediments in non-glacial, marine Cryogenian sediments (Giddings and Wallace, 2009a, b; Wallace et al., 2019). In particular, this authigenic dolomite is similar in appearance, distribution and isotopic composition to the overlying Sturtian 'cap' carbonate of the Tindelpina Shale Member: a ~5–15 m dolomite unit which consists of finely-laminated disseminated clastic material cemented by non-bright-luminescent dolomite in the northern Flinders Ranges (Giddings and Wallace, 2009a). This unit is also present at Holowilena South and contains ~60–87% carbonate (Table S1). Strong sedimentological and geochemical similarities between the bedded dolomite units of the Yudnamutana Subgroup and a variety of non-glacial Neoproterozoic dolomite marine hardgrounds (e.g. impure dolomicrite composition, graded beds, Wallace et al., 2019) supports a common marine authigenic origin for these glacial dolomite units.

More tenuously, if non-glacial deep water dolomite and syn-glacial dolomite from this basin did precipitate from a fluid with a similar carbon isotopic signature (e.g. whether reflecting solely Cryogenian marine DIC, or a mix of DIC and remineralised organic carbon), it is possible to speculate that seawater $\delta^{13}C$ composition was not significantly affected by glaciation (c.f. Hoffman et al., 1998; 2017). Importantly, these carbon isotope results are not representative of mantle $\delta^{13}C$ signatures as interpreted for oceans under 'snowball Earth' conditions in the most extreme version of the theory (~-5‰; c.f. Hoffman et al., 1998). Therefore if these Yudnamutana Subgroup carbon isotope results do at least partially reflect the marine DIC reservoir, it suggests that Sturtian marine conditions in this ocean basin were not dominated solely by carbon input from submarine volcanism in the absence of biological activity and continental input.

5.3 Carbonate in other Sturtian successions

This article is protected by copyright. All rights reserved

Author Manuscript

The close association of Neoproterozoic glacial deposits with (typically dolomitic) carbonates, including those interbedded with glacial strata, has long been recognised (e.g., Howchin, 1918). Carbonate also occurs in other Sturtian sequences globally, and in some successions is present as a major component of the glacial lithology (e.g. Pedrosa-Soares et al., 2011; Fairchild et al., 2018; Lechte et al., 2018; Macdonald et al., 2018; Mackey et al., 2020). In many of these Sturtian successions, carbonate in matrix material is distinct both geochemically and sedimentologically from many detrital carbonate clasts, which may show distinctive carbonate lithologies (e.g. Mackey et al., 2020).

A compilation of Sturtian stratigraphic successions which contain carbonate are included in Table 1 and are discussed in detail here. Comparison between the observations of syn-glacial carbonate in the Adelaide Fold Belt with global successions highlights that carbonate lithologies are present and sometimes common in Sturtian glacial sediments globally. Both dolomite and limestone lithologies occur in global Sturtian sequences, though dolomite appears to be more common (Table 1). While it is difficult to directly correlate Sturtian successions globally, carbonate does appear to be present in a variety of glacio-marine facies, and can occur throughout the preserved record of glaciation. In particular, the occurrence of dolomite in many of these glacial units suggests that carbonate saturation and Mg cycling is maintained in marine environments during glaciation.

Dolomite beds are reported from within the lower Port Askaig Formation, Scotland, associated with diamictite facies deposited during the onset and early stages of the Sturtian glaciation (Spencer, 1971; Fairchild et al., 2018). Spencer (1971) considered that a detrital origin for these dolomite beds was unlikely due to a lack of a suitable source in underlying strata, and suggested that the dolomite is not the product of late-stage dolomitization, instead preferring an authigenic (or early diagenetic) origin. These dolomitic lithologies may be graded and intraclastic, with some beds having sandy, intraclastic erosional bases and fining up to dolomite with an eroded top, with dolomite intraclasts (Fairchild et al., 2018). In light of the sedimentological observations of the Yudnamutana Subgroup in this study, evidence of syn-sedimentary erosion and the formation of dolomite intraclasts from the Port Askaig Formation implies that dolomite may have similarly precipitated early (e.g. during sedimentation). Ferroan dolomite concretions are also present in diamictites and siltstones of the Port Askaig Formation in Islay, Scotland (Spence, Le Heron & Fairchild, 2016). Carbon isotope compositions of the bedded dolomites of the Port Askaig Formation cluster around ~

This article is protected by copyright. All rights reserved

Author Manuscript

506 0 to 1‰, (Fairchild et al., 2018). By contrast, dolomite clasts within the Port Askaig
507 Formation show a much wider range of $\delta^{13}C$ values ranging from approximately -3 to +2 ‰
508 (Fairchild et al., 2018). Significantly, this observation shows that in addition to the
509 Yudnamutana Subgroup, other Sturtian carbonate-rich sediments have been demonstrated to
510 feature a distinctly different isotopic composition from detrital carbonate components.
511
512 Sturtian units from North America also contain substantial carbonate-bearing glacial
513 lithologies. In northwestern Canada, the Rapitan Group comprises the glacial deposits of the
514 Sturtian glaciation, and the correlative Eagle Creek Formation of the Ogilvie Mountains,
515 Yukon, is often dominated by dolomite (Macdonald et al., 2018). In particular, in the Eagle
516 Creek Formation features yellow dolomite matrix material is present in a range of lithologies
517 including diamictite, conglomerate and siltstone (Macdonald et al., 2018). One laminated
518 microbial dolomite bed and abundant dolomite grainstone beds are also reported from the
519 syn-glacial Eagle Creek Formation, associated with ripple cross lamination and dropstones
520 (Macdonald et al., 2018). In the USA, Lechte et al. (2018) observed rare beds of dolomite in
521 the upper Kingston Peak Formation (KP3) at Sperry Wash, California, associated with shale
522 and ironstones (Fig. S2). These beds are buff-yellow, finely-crystalline dolomite, and may be
523 nodular in appearance. Yellow- to buff-weathering dolomitic sandstone beds are also
524 common; these are typically graded, and can be capped by ripple cross lamination suggestive
525 of a turbidite origin (Lechte et al., 2018). In contrast, abundant grey dolomite clasts are also
526 present in diamictite, but are sedimentologically distinct (i.e. pure, grey ooidal and microbial
527 carbonate lithologies), and are likely to be derived from the underlying Beck Spring
528 Dolomite (Lechte et al., 2018).
529
530 While the Neoproterozoic glacial stratigraphy of Brazil suffers from a paucity of direct
531 geochronological constraints, in the Araçuaí orogen, Babinski et al. (2012) described the
532 Neoproterozoic glaciomarine (early Sturtian?) Serra do Catuni Formation as containing
533 diamictite with a carbonate matrix. Sandstone containing carbonate is also present (Babinski
534 et al., 2012). Overlying these glacial deposits, Pedrosa-Soares et al., (2011) reported rare
535 carbonate in glaciomarine Lower Chapada Acauã Formation, tentatively suggested to
536 represent a late phase of Sturtian glaciation, including a ~20m thick limestone lens
537 interbedded with shales with isolated outsized clasts, stratigraphically overlain and underlain
538 by diamictites (Pedrosa-Soares et al., 2011). Further, the Vazante Group of the Saõ Francisco
539 Basin has two glacial units present containing carbonate lithologies, which may correlate

This article is protected by copyright. All rights reserved

Author Manuscript

with the Sturtian glaciation (Olcott, Sessions, Corsetti, Kaufman & De Oliviera, 2005; Pedrosa-Soares et al., 2011). The upper unit of these glacial successions is the Serra do Poço Verde Formation, which contains carbonate diamictites with dolomite clasts that are associated with dropstone-bearing black shales with glendonite (pseudomorphs of the mineral ikaite which forms in near-freezing conditions; Olcott et al., 2005; Pedrosa-Soares et al., 2011).

Glacially-associated carbonates have been documented in Svalbard (Mackey et al. 2020). In the Petrovbreen Member of the Elbobreen Formation, which is considered to represent early glacial facies of the Sturtian glaciation of Svalbard (e.g. Fairchild et al., 1989), dolomite is present as matrix dolomicrite in homogeneous or laminated beds, and in diamictite (Mackey et al., 2020). Diamictites can be composed of up to 70% dolomite as well as in small and large clasts (Fairchild et al., 1989; Mackey et al., 2020). Glacial dolomicrite has a carbon and oxygen composition (mean $\delta^{13}C$ -4.4 ‰; mean $\delta^{18}O$ +5 ‰) generally distinct from pre-glacial carbonates of this succession, but overlaps with a small proportion of carbonates in detrital clasts (Mackey et al., 2020). Some clasts show sedimentological similarity to the underlying carbonates, whereas others appear to be derived from reworking of dolomicrite in the glacial environment (Mackey et al., 2020). Mackey et al. (2020) interpret the Petrovbreen Member dolomicrite as reflecting early dolomite precipitation in the glacial environment based on their distinct isotopic composition, low reconstructed clumped isotopic temperatures of precipitation (26 ± 10°C), fine crystal size and soft sediment deformation.

In northern Namibia, the Sturtian Chuos Formation variably features rare beds of laminated, micritic limestone and dolomite, including a laterally continuous limestone unit, interbedded with glacial diamictite intervals (Hoffman et al. 2021). These syn-glacial carbonate beds can be graded, or feature stratigraphic variation in their carbonate content (Hoffman et al. 2021). The stable isotope composition of the micritic dolomite and limestone beds ($\delta^{13}C$ between -1.88 to -9.25 ‰; $\delta^{18}O$ between -7.86 and -14.69‰) is distinct from the carbonates of the underlying Ugab Subgroup (Hoffman et al. 2021).

In South China, Yu et al. (2017) document dolomitic lithologies within the Tiesi'ao Formation in Eastern Guizhou Province, South China, considered correlative with the Sturtian glaciation. The upper diamictite units of this formation have a dolomitic micrite matrix; Yu et al. (2017) interpreted this diamictite as deglacial, with carbonate sourced from

This article is protected by copyright. All rights reserved

Author Manuscript

574 the underlying, pre-glacial carbonate and calcareous shale units. In the southern Guizhou
575 province and northern Guangxi, the Jiangkou Group–comprising the Chang'an and Fulu
576 Formations–has also been tentatively correlated to the Sturtian glaciation. The Liangjiehe
577 Member of the Fulu Formation features a thick succession of arkosic arenites that have beds
578 of micritic dolomite, dolomitic sandstone and lensoidal dolomite mounds (Zhou, Du, Yan,
579 Zhang & Yin, 2007; Zhang, Chu and Feng, 2011). This association of the Sturtian glacial
580 deposits with carbonate facies was also documented in the Hunan Province (Dobrzinski,
581 Bahlburg, Strauss & Zhang, 2004). The dolomite and dolomitic sandstones of the Fulu
582 Formation display $\delta^{13}C$ values ranging from -2.86 ‰ to -1.87 ‰ and were interpreted to have
583 been deposited as cold spring carbonate deposits (Zhou et al., 2007).
584
585 In summary, in addition to the Australian Neoproterozoic successions, carbonate
586 lithologies—dominantly dolomitic—are preserved globally in Sturtian glacial sequences
587 associated with a range of glaciomarine paleoenvironments. In some successions, carbonate-
588 rich lithologies even dominate the stratigraphy, though in many cases carbonate forms a
589 minor to moderate proportion of the glacial lithology. Similar to the Sturtian succession in
590 South Australia, dolomite appears to be found in a range of glacio-marine environments, and
591 can form matrix and clast material in bedded, laminated and diamictite glacio-marine facies.
592 More recent studies of these carbonates (e.g. Mackey et al., 2020) interpret some matrix
593 dolomite as syn-glacial dolomite precipitation, consistent with the sedimentological data from
594 this study. Finally, in addition to dolomitic glacial sediments, dolomitic or calcareous cap
595 carbonates often also overlie Sturtian glacial deposits in many global localities and may reach
596 tens of metres in thickness (e.g. Giddings and Wallace, 2009a; Yu et al., 2017; Hoffman et
597 al., 2017).
598
599 More broadly, while dolomite does not precipitate readily from modern seawater in open
600 marine settings (e.g. Land, 1998), there is now evidence to suggest that dolomite commonly
601 formed in synsedimentary marine conditions during the Neoproterozoic (e.g. Tucker, 1982;
602 Hood and Wallace 2012; Wood et al., 2017; Hood and Wallace, 2018; Shuster et al., 2018;
603 Hu et al., 2020). Neoproterozoic carbonates are commonly composed of fabric-preserving
604 dolomite (e.g. Tucker, 1982). In addition, marine cements from the Precambrian commonly
605 preserve primary cathodoluminescent growth zonation and have optical characteristics that
606 indicate direct precipitation of dolomite from seawater (e.g. Hood and Wallace, 2012; Shuster
607 et al., 2018; Hu et al., 2020). Seawater conditions which may have facilitated dolomite

This article is protected by copyright. All rights reserved

Author Manuscript

precipitation during this time include marine anoxia (ferruginous conditions), high carbonate supersaturation, and high Mg/Ca ratios (see discussion in Hood and Wallace, 2012; Cantine et al., 2020).

6. Carbon cycling during Neoproterozoic glaciation

The observation of syn-sedimentary dolomite precipitation throughout, and immediately following the ~50 My Sturtian glaciation is inconsistent with the hypothesis that carbonate dissolution would have been favoured during glaciation as proposed in the original 'snowball Earth' scenario (attributed to high dissolved CO_2, Hoffman et al., 1998) and many subsequent 'hard snowball' models (e.g., Hoffman et al., 2017; Le Hir et al., 2008). Carbonate lithologies, which are dominated by a dolomite mineralogy, are also common in a range of locations and glacial facies in Australia and globally. This sedimentological data suggests there must have been a high enough carbonate saturation state for Sturtian syn-glacial seawater to support carbonate precipitation. Models for syn-glacial seawater chemistry must further be able to account for the precipitation of dolomite, which is generally associated with higher Mg/Ca fluid conditions (as opposed to a scenario where the continued removal of Mg^{2+} by oceanic crustal alteration would result in low oceanic Mg/Ca: Hardie, 1996; Hoffman et al., 1998; Le Hir et al., 2008; Coogan and Gillis, 2018). Thus, the abundant syn-glacial carbonate in Sturtian successions—and the occurrence of marine dolomite throughout and after glaciation—appears to be inconsistent with key predictions of the snowball Earth hypothesis. Evidence of dolomite precipitation during the Sturtian implies the need to re-assess the Neoproterozoic syn-glacial carbon cycle.

6.1 Geochemical modelling

In order to explore the relationships between observations of syn-glacial carbonate precipitation, the regional and global distribution of glacial carbonate units, seawater chemical conditions, and the mineralogy of Sturtian cap carbonates, we performed a series of snowball Earth simulations using PreCOSCIOUS (Penman and Rooney, 2019) (Fig. 9). PreCOSCIOUS is a 3-box (atmosphere, surface and deep ocean) geochemical model of the Precambrian carbon and silica cycles including processes crucial to understanding the evolution of Sturtian seawater chemistry. Modelled processes include: chemical weathering feedbacks; inorganic $CaCO_3$ and SiO_2 burial; air-sea gas exchange; volcanic CO_2 degassing; and a CO_2 greenhouse effect. A full description of the PreCOSCIOUS model parameters is given in Penman and Rooney (2019). The PreCOSCIOUS model was modified for the

This article is protected by copyright. All rights reserved

Author Manuscript

present purpose to include seawater [Ca] and [Mg] as additional tracers, with fluxes representing carbonate and silicate weathering, carbonate burial, and Mg-Ca exchange by seafloor alteration and dissolution of carbonates in seawater (whenever calcium carbonate saturation state, $\Omega < 1$; see Supplementary Information for details on model code.)

Equilibrium constants for carbonate minerals were modified based on seawater [Mg] and [Ca] (Zeebe and Tyrrell, 2019). The runs presented in the main text assume that carbonate minerals precipitate according to the solubility and precipitation dynamics of calcite, including accounting for the effects of colder temperatures during glaciation (after Penman & Rooney 2019). Sensitivity tests which consider the solubilities of dolomite and magnesite as well as different inorganic precipitation thresholds demonstrate that our main conclusions are insensitive to those details of how carbonate precipitation is governed (Supplementary Information). Over the long timescales of the model runs (millions of years), the main factor that influences the carbonate burial rate (i.e. the only process removing alkalinity from the ocean) is the weathering rate, which is the only process adding alkalinity to the ocean.

Sedimentological observations were used to constrain model parameters through the Sturtian glaciation. In the model setup, high Mg/Ca ratios are assumed for pre-glacial seawater (~5.2), consistent with tectonic modelling studies (Hardie, 2003) and petrographic records of the dominance of aragonite and dolomite marine carbonate mineralogy through the Tonian-Cryogenian (Hood and Wallace, 2018). Carbonate precipitation and carbonate weathering are set at a Mg:Ca ratio of 1, indicating dolomitic lithologies for all weathered and precipitating carbonates in the model. This is consistent with sedimentological observations of syn-glacial dolomite precipitation in this study, as well as the dominantly dolomitic Sturtian and underlying Precambrian stratigraphy in South Australia and elsewhere (Section 5; Preiss, 1987; Cantine et al., 2020). This is also in line with evidence for marine and mimetic dolomite precipitation during much of the Neoproterozoic (Tucker, 1982; Hood and Wallace, 2012; Wood et al., 2017; Hood and Wallace, 2018; Shuster et al., 2018; Hu et al., 2020; see compilation in Cantine et al., 2020)

In the model, hydrothermal alteration exchanges (removes) Mg^{2+} and (releases) Ca^{2+} at a rate of 1.5×10^{12} moles per year (Higgins and Schrag, 2015). In order to offset this Mg^{2+} loss and Ca^{2+} addition and balance the Mg^{2+} and Ca^{2+} budgets over long time scales, the Mg/Ca ratio associated with silicate weathering is >1. This Mg enrichment factor was set to balance the

This article is protected by copyright. All rights reserved

Author Manuscript

676 Mg^{2+} and Ca^{2+} cycles at the equilibrium point of the long-term carbon cycle: e.g. when CO_2
677 consumption by silicate weathering perfectly balances volcanic CO_2 degassing (rate= 5
678 Tmol/year: Penman and Rooney, 2019), the Mg^{2+} loss from hydrothermal alteration is
679 perfectly balanced by elevated Mg^{2+} derived from silicate weathering (and vice versa for
680 Ca^{2+}).
681
682 The PreCOSCIOUS (Penman and Rooney, 2019) snowball Earth scenario implements a
683 simple forcing to represent global glaciation, during which all chemical weathering halts,
684 allowing atmospheric pCO_2 to increase until a deglaciation threshold (0.12 bar, Caldeira and
685 Kasting, 1992) is crossed, which triggers deglaciation. However, this scenario fails to satisfy
686 key constraints imposed by our new observations for the Sturtian glaciation. In the absence of
687 any chemical weathering to supply alkalinity, the marine carbonate saturation state plummets
688 and carbonate burial ceases—i.e. the ocean is more conducive to the dissolution of carbonate;
689 Fig. 9a)—which is inconsistent with the syn-glacial dolomite precipitation documented here.
690 In addition, due to ongoing Mg consumption and Ca release by seafloor alteration (Hardie,
691 1996; Coogan and Gillis, 2018) in the absence of any Mg input from carbonate and silicate
692 weathering, seawater Mg/Ca declines significantly throughout the glacial interval (Fig. 9a).
693 This results in [Ca]>>[Mg] upon deglaciation, seemingly inconsistent with the common
694 dolomitic mineralogy of the Sturtian syn-glacial and cap carbonates (e.g. Giddings and
695 Wallace, 2009a; Yu et al., 2017).
696
697 An important corollary of the PreCOSCIOUS snowball Earth model output (Penman and
698 Rooney, 2019) is that in the total absence of silicate weathering as a significant CO_2 sink
699 (with a standard deglaciation CO_2 threshold, 0.12 bar: Caldeira and Kasting, 1992),
700 deglaciation occurs after only ~ 7 My (Penman and Rooney, 2019). This duration is
701 consistent with geochronologic constraints on the Marinoan glaciation (~4–15 My) but it is
702 not consistent with the longer ~57 My Sturtian glaciation (Rooney et al., 2015). The most
703 straightforward way to obtain a longer glacial interval is to impose a higher pCO_2 threshold
704 for deglaciation (e.g. Pierrehumbert, 2004). For example, to approach a ~40 My glaciation,
705 PreCOSCIOUS requires a very high deglaciation pCO_2 threshold of 0.8 bar ("high threshold
706 scenario", Fig. 9a). However, imposing a high deglaciation threshold results in carbonate
707 dissolution during glaciation–rather than the carbonate precipitation interpreted here–as well
708 as relatively stratigraphically thick cap carbonates. This contrasts with their preservation in
709 the sedimentary record, which is commonly less than 1m and up to ~20 m for the Sturtian cap

This article is protected by copyright. All rights reserved

Author Manuscript

carbonates (e.g., Giddings and Wallace, 2009a; Hoffman et al., 2017; Yu et al., 2017). In order to address these issues, we explore modifications to the PreCOSCIOUS scenario to account for the observed syn-glacial precipitation of dolomite and more accurately model the longer duration of the Sturtian glaciation (Fig. 9).

One way to allow carbonate precipitation and obtain a long (~50 My) glacial duration in the PreCOSCIOUS model is to slow the rate of pCO_2 rise by allowing its consumption by some degree of limited silicate weathering. The rate of silicate weathering must be limited to less than the volcanic degassing flux: if CO_2 consumption by silicate weathering is allowed to balance degassing, CO_2 stabilizes, and the deglaciation threshold is never reached. We prescribe two different scenarios that allow limited chemical weathering during the glacial period and allow carbonate precipitation (Fig. 9b-c). In the first (the "constant weathering" scenario, Fig. 9b), a weathering flux equal to 80% of the volcanic degassing flux was imposed. This rate was tuned to obtain a glacial duration close to estimates for the Sturtian glaciation (Rooney et al., 2015). In the second (the "weak weathering feedback" scenario, Fig. 9c), weathering rate is calculated as a function of atmospheric pCO_2 using the same relationship used outside the glacial interval ($F_w = F_{vc}*(pCO_2/pCO_{2i})^{NSi}$, where F_{vc} is the volcanic degassing rate, pCO_{2i} is equilibrium pCO_2, and N_{Si} is a rate constant, here 0.5), but the entire relationship is scaled down to 9% (e.g. $F_w = 0.09 *F_{vc}*(pCO_2/pCO_{2i})^{NSi}$, tuned for appropriate Sturtian glacial duration). Importantly, both of these scenarios can replicate the ~50 My length of the Sturtian, along with the precipitation of dolomite during and after glaciation.

6.2 Possible sources of alkalinity

The partial drawdown of atmospheric CO_2—and the associated precipitation of authigenic syn-sedimentary dolomite—during snowball Earth can be explained by ongoing chemical weathering, allowing alkalinity input into glacial oceans. Possible sources of syn-glacial weathering in these scenarios include continental weathering of subglacial bedrock (i.e., meltwater delivery of alkalinity), subaerially exposed silicate rocks and non-glaciated continental crust (i.e., riverine delivery). Alternatively, alkalinity could be generated from the marine weathering of detrital marine sediments or basaltic seafloor crust (Le Hir et al., 2008; Gernon, Hincks, Tyrrell, Rohling & Palmer, 2016). Resolving these alkalinity sources has important implications for the syn-glacial carbon cycle and climate. Critically, this

Author Manuscript

This article is protected by copyright. All rights reserved

743 weathering process must also actively input Mg^{2+} into the ocean over losses to Mg-Ca
744 exchange with the oceanic crust.
745
746 Marine basaltic crustal weathering may be a source of alkalinity, though it is largely self-
747 buffering, and alkalinity release can be negligible due to local carbonate precipitation in
748 crustal vein systems (Le Hir et al., 2008). However, high and low-temperature basaltic crustal
749 weathering is generally considered a Mg sink (Hardie, 1996; Coogan and Gillis, 2018). While
750 hyaloclastite alteration (palagonitization) can release alkalinity and Mg^{2+} into seawater
751 (Gernon et al., 2016), it can also result in removal of Mg^{2+} from seawater (Stroncik and
752 Schmincke, 2001). Further, hyaloclastite alteration occurs in association with increased ridge
753 volcanism; a scenario generally resulting in increased Mg^{2+} removal from seawater (Hardie,
754 1996). Importantly, rates of marine (low-T) weathering of the seafloor crust and detrital
755 reactive silicates would likely have been slowed by both the low temperatures of glacial
756 oceans as well as reduced siliciclastic input from widespread ice cover. However, it is
757 possible that cold ocean temperatures during glaciation may have decreased Mg^{2+} removal
758 from the oceans via diminished authigenic clay formation (Higgins and Schrag, 2015). In
759 sum, although there are large uncertainties in all of these marine weathering fluxes, every
760 scenario requires continentally sourced Mg^{2+} input in order to replenish Mg^{2+} loss over ~50
761 My. Therefore, while marine weathering processes may have contributed to alkalinity
762 generation during the Sturtian glaciation, it is more likely that continental silicate weathering
763 played a significant role in Mg cycling, requiring liquid water on the continents. According to
764 our modelling results and geological observations, this continental supply of alkalinity needs
765 to be reconciled with climate models for the Sturtian glaciation.
766
767 The chemical weathering of the continents and the associated supply of alkalinity to the
768 oceans during snowball Earth may suggest the presence of (at least temporary) temperate
769 land conditions and associated riverine fluxes despite high planetary albedo due to
770 widespread ice coverage (see Paradise et al. 2019). It is also possible that polythermal ice
771 sheets could have supplied glacial meltwater to the oceans during the Sturtian glaciation (e.g.,
772 Hoffman et al. 2017; Lechte et al. 2019), leading to ongoing chemical weathering and a
773 continental alkalinity flux. Regardless of the ultimate alkalinity source, a small degree of
774 continental silicate weathering during glaciation (Fig. 9b,c) can better explain both alkalinity
775 and Mg^{2+} input into glacial oceans, accounting for observed syn-glacial dolomite

Author Manuscript

This article is protected by copyright. All rights reserved

776 precipitation in the Adelaide Fold Belt and globally. Importantly, this process can therefore
777 help explain the longevity of the Sturtian glaciation.
778
779 **6. Implications and Conclusions**
780 According to our modelling results, the 'snowball Earth' hypothesis sensu stricto (Hoffman
781 et al., 1998; Hoffman et al., 2017), which invokes a near-total shutdown of continental
782 weathering, cannot simultaneously account for observed syn-glacial carbonate, the marine
783 dolomite mineralogy of the syn- and post-glacial carbonates, and the long duration of the
784 Sturtian glaciation. However, our model scenarios that include syn-glacial silicate weathering
785 (Fig. 9b-c) are more consistent with the sedimentology and chronology of Sturtian
786 successions than are either the PreCOSCIOUS snowball Earth scenario (Penman and
787 Rooney, 2019) or the traditional higher deglaciation threshold scenario (e.g. Fig. 9a). With a
788 limited supply of alkalinity, carbonate supersaturation is maintained throughout the glacial
789 period (immediately in the constant flux scenario, and only after ~2 million years of CO_2 rise
790 in the reduced weathering feedback scenario), allowing some precipitation of syn-glacial
791 carbonate. With continental weathering providing a crucial source of Mg^{2+} throughout the
792 glaciation, the drawdown of seawater Mg^{2+} is far less pronounced, resulting in [Mg] > [Ca]
793 upon deglaciation, consistent with the dolomite mineralogy typical of Cryogenian cap
794 carbonates. A limited weathering scenario also supports relatively stratigraphically thinner
795 post-glacial cap carbonates, as indicated by the reduced extent of carbonate burial after
796 deglaciation (Fig. 9b,c).
797
798 These observations and insights add to our understanding of environmental conditions during
799 one of Earth's most severe ice ages: the Sturtian glaciation. There has been significant debate
800 about the severity of the Cryogenian glaciations, including the extent and thickness of ocean
801 ice coverage (e.g. 'hard snowball' versus 'slushball' conditions; for example see discussion
802 in Hyde et al., 2000; Hoffman et al., 2017). We suggest the hydrological cycle and
803 continental chemical weathering processes remained active during the Sturtian glaciation.
804 This continental weathering, alkalinity supply and subsequent carbonate burial would have
805 slowed the rate of atmospheric CO_2 build-up, delaying deglaciation for tens of millions of
806 years. The persistence of marine carbonate precipitation throughout the Sturtian glaciation
807 suggests that the impact of low-latitude glaciation on the carbon and hydrological cycles—
808 while clearly severe—may not have been as extreme as previously suggested. However,
809 building on the foundation of decades of research considering Neoproterozoic climate change

This article is protected by copyright. All rights reserved

Author Manuscript

(e.g., Harland, 1964; Kirschvink, 1992; Hoffman et al., 1998; Hoffman et al., 2017), we suggest that further detailed geological observations are necessary to more precisely develop our understanding of Earth's geological record of climate change.

References

Babinski, M., Pedrosa-Soares, A., Trindade, R. I. F. d., Martins, M., Noce, C. M., & Liu, D. (2012). Neoproterozoic glacial deposits from the Araçuaí orogen, Brazil: Age, provenance and correlations with the São Francisco craton and West Congo belt. Gondwana Research, 21(2-3), 451-465.

Budyko, M.I. (1969). The effect of solar radiation variations on the climate of the Earth. Tellus, 21, 611–619.

Caldeira, K., & Kasting, J. F. (1992). The life span of the biosphere revisited. Nature, 360(6406), 721-723.

Canfield, D. E., Poulton, S. W., Knoll, A. H., Narbonne, G. M., Ross, G., Goldberg, T., & Strauss, H. (2008). Ferruginous conditions dominated later Neoproterozoic deep-water chemistry. Science, 321(5891), 949-952.

Cantine, M. D., Knoll, A. H., & Bergmann, K. D. (2020). Carbonates before skeletons: A database approach. Earth-Science Reviews, 201, 103065.

Coogan, L. A., & Gillis, K. M. (2018). Low-temperature alteration of the seafloor: Impacts on ocean chemistry. Annual Review of Earth and Planetary Sciences, 46, 21-45.

Cox, G. M., Isakson, V., Hoffman, P. F., Gernon, T. M., Schmitz, M. D., Shahin, S., . . . Mitchell, R. N. (2018). South Australian U-Pb zircon (CA-ID-TIMS) age supports globally synchronous Sturtian deglaciation. Precambrian Research, 315, 257-263.

Crossing, A. R., & Gostin, V. A. (1994). Isotopic signatures of carbonates associated with Sturtian (Neoproterozoic) glacial facies, central Flinders Ranges, South Australia: Cambridge: Cambridge University Press.

Defliese, W. F. (2021). The impact of Snowball Earth glaciation on ocean water $\delta^{18}O$ values. Earth and Planetary Science Letters, 554, 116661.

Dobrzinski, N., Bahlburg, H., Strauss, H., & Zhang, Q.-R. (2004). Geochemical climate proxies applied to the Neoproterozoic glacial succession on the Yangtze Platform, South China (Vol. 146): American Geophysical Union Monograph Series.

Fairchild, I. J., & Hambrey, M. J. (1984). The Vendian succession of northeastern Spitsbergen: Petrogenesis of a dolomite-tillite association. Precambrian Research, 26(2), 111-167.

This article is protected by copyright. All rights reserved

Author Manuscript

Fairchild, I. J., Hambrey, M. J., Spiro, B., & Jefferson, T. H. (1989). Late Proterozoic glacial carbonates in northeast Spitsbergen: new insights into the carbonate–tillite association. Geological Magazine, 126(5), 469-490.

Fairchild, I. J., Spencer, A. M., Ali, D. O., Anderson, R. P., Anderton, R., Boomer, I., . . . Howe, J. (2018). Tonian-Cryogenian boundary sections of Argyll, Scotland. Precambrian Research, 319, 37-64.

Frank, T. D., & Fielding, C. R. (2003). Marine origin for Precambrian, carbonate-hosted magnesite? Geology, 31(12), 1101-1104.

Gernon, T. M., Hincks, T. K., Tyrrell, T., Rohling, E. J., & Palmer, M. R. (2016). Snowball Earth ocean chemistry driven by extensive ridge volcanism during Rodinia breakup. Nature Geoscience, 9(3), 242-248.

Giddings, J. A., & Wallace, M. W. (2009)a. Sedimentology and C-isotope geochemistry of the 'Sturtian'cap carbonate, South Australia. Sedimentary Geology, 216(1-2), 1-14.

Giddings, J. A., & Wallace, M. W. (2009)b. Facies-dependent δ13C variation from a Cryogenian platform margin, South Australia: Evidence for stratified Neoproterozoic oceans? Palaeogeography, Palaeoclimatology, Palaeoecology, 271(3-4), 196-214.

Grotzinger, J. P., & James, N. P. (2000). Precambrian carbonates: Evolution of understanding (Vol. 67): SEPM Special Publication.

Halverson, G. P. (2011). Glacial sediments and associated strata of the Polarisbreen Group, northeastern Svalbard. Geological Society, London, Memoirs, 36(1), 571-579.

Hardie, L. A. (1996). Secular variation in seawater chemistry: An explanation for the coupled secular variation in the mineralogies of marine limestones and potash evaporites over the past 600 my. Geology, 24(3), 279-283.

Hardie, L. A. (2003). Secular variations in Precambrian seawater chemistry and the timing of Precambrian aragonite seas and calcite seas. Geology, 31(9), 785-788.

Harland, W. B. (1964). Critical evidence for a great infra-Cambrian glaciation. Geologische Rundschau, 54(1), 45-61.

Higgins, J. A., & Schrag, D. P. (2015). The Mg isotopic composition of Cenozoic seawater–evidence for a link between Mg-clays, seawater Mg/Ca, and climate. Earth and Planetary Science Letters, 416, 73-81.

Hill, A. C., & Walter, M. R. (2000). Mid-Neoproterozoic (~ 830–750 Ma) isotope stratigraphy of Australia and global correlation. Precambrian Research, 100(1-3), 181-211.

This article is protected by copyright. All rights reserved

Author Manuscript

Hoffman, P. F., Abbot, D. S., Ashkenazy, Y., Benn, D. I., Brocks, J. J., Cohen, P. A., . . . Warren, S. G. (2017). Snowball Earth climate dynamics and Cryogenian geology-geobiology. Science Advances, 3(11), e1600983.

Hoffman, P. F., Kaufman, A. J., Halverson, G. P., & Schrag, D. P. (1998). A Neoproterozoic snowball earth. science, 281(5381), 1342-1346.

Hoffman, P.F., Halverson, G.P., Schrag, D.P., Higgins, J.A., Domack, E.W., Macdonald, F.A., Pruss, S.B., Blättler, C.L., Crockford, P.W., Hodgin, E.B. and Bellefroid, E.J. (2021). Snowballs in Africa: sectioning a long-lived Neoproterozoic carbonate platform and its bathyal foreslope (NW Namibia). Earth-Science Reviews, 103616.

Hood, A. v. S., & Wallace, M. W. (2012). Synsedimentary diagenesis in a Cryogenian reef complex: Ubiquitous marine dolomite precipitation. Sedimentary Geology, 255, 56-71.

Hood, A. v. S., & Wallace, M. W. (2018). Neoproterozoic marine carbonates and their paleoceanographic significance. Global and Planetary Change, 160, 28-45.

Howchin, W. (1918). The Geology of South Australia. Adelaide: Education Department.

Hu, Y., Cai, C., Liu, D., Pederson, C. L., Jiang, L., Shen, A., & Immenhauser, A. (2020). Formation, diagenesis and palaeoenvironmental significance of upper Ediacaran fibrous dolomite cements. Sedimentology, 67(2), 1161-1187.

Hulsemann, J. (1966). On the routine analysis of carbonates in unconsolidated sediments. Journal of Sedimentary Research, 36(2), 622-625.

Hyde, W. T., Crowley, T. J., Baum, S. K., & Peltier, W. R. (2000). Neoproterozoic 'snowball Earth' simulations with a coupled climate/ice-sheet model. Nature, 405(6785), 425-429.

James, N. P. (1997). The Cool-Water Carbonate Depositional Realm. In N. P. James & J. A. D. Clarke (Eds.), Cool-Water Carbonates (Vol. 56, pp. 1-20): SEPM Society for Sedimentary Geology.

Kirschvink, J. L. (1992). Late Proterozoic low-latitude global glaciation: the snowball Earth: Cambridge University Press.

Land, L. S. (1998). Failure to Precipitate Dolomite at 25 C from Dilute Solution Despite 1000-Fold Oversaturation after 32 Years. Aquatic Geochemistry, 4(3-4), 361-368.

Le Heron, D. P., Busfield, M. E., & Collins, A. S. (2014). Bolla Bollana boulder beds: A Neoproterozoic trough mouth fan in South Australia? Sedimentology, 61(4), 978-995.

This article is protected by copyright. All rights reserved

Author Manuscript

Le Heron, D. P., Cox, G., Trundley, A., & Collins, A. S. (2011). Two Cryogenian glacial successions compared: Aspects of the Sturt and Elatina sediment records of South Australia. Precambrian Research, 186(1-4), 147-168.

Le Hir, G., Goddéris, Y., Donnadieu, Y., & Ramstein, G. (2008). A geochemical modelling study of the evolution of the chemical composition of seawater linked to a" snowball" glaciation.

Lechte, M. A., & Wallace, M. W. (2015). Sedimentary and tectonic history of the Holowilena Ironstone, a Neoproterozoic iron formation in South Australia. Sedimentary Geology, 329, 211-224.

Lechte, M. A., Wallace, M. W., Hood, A. v. S., Li, W., Jiang, G., Halverson, G. P., . . . Planavsky, N. J. (2019). Subglacial meltwater supported aerobic marine habitats during Snowball Earth. Proceedings of the National Academy of Sciences, 116(51), 25478-25483.

Lechte, M. A., Wallace, M. W., Hood, A. v. S., & Planavsky, N. (2018). Cryogenian iron formations in the glaciogenic Kingston Peak Formation, California. Precambrian Research, 310, 443-462.

Macdonald, F. A., Schmitz, M. D., Strauss, J. V., Halverson, G. P., Gibson, T. M., Eyster, A., . . . Crowley, J. L. (2018). Cryogenian of Yukon. Precambrian Research, 319, 114-143.

Mackey, T. J., Jost, A. B., Creveling, J., & Bergmann, K. D. (2020). Temperature and Hydrologic Cycle Constraints on Snowball Earth Environments. Earth and Space Science Open Archive. doi:doi:10.1002/essoar.10501936.1

McKirdy, D. M., Burgess, J. M., Lemon, N. M., Yu, X., Cooper, A. M., Gostin, V. A., . . . Both, R. A. (2001). A chemostratigraphic overview of the late Cryogenian interglacial sequence in the Adelaide Fold-Thrust Belt, South Australia. Precambrian Research, 106(1-2), 149-186.

O'Neil, J. R. (1968). Hydrogen and oxygen isotope fractionation between ice and water. The Journal of Physical Chemistry, 72(10), 3683-3684.

Olcott, A. N., Sessions, A. L., Corsetti, F. A., Kaufman, A. J., & De Oliviera, T. F. (2005). Biomarker evidence for photosynthesis during Neoproterozoic glaciation. Science, 310(5747), 471-474.

Paradise, A., Menou, K., Valencia, D. and Lee, C. (2019) Habitable snowballs: Temperate land conditions, liquid water, and implications for CO2 weathering. Journal of Geophysical Research: Planets, 124(8), 2087-2100.

This article is protected by copyright. All rights reserved

Author Manuscript

Pedrosa-Soares, A. C., De Campos, C. P., Noce, C., Silva, L. C., Novo, T., Roncato, J., . . . Dantas, E. (2011). Late Neoproterozoic-Cambrian granitic magmatism in the Araçuaí orogen (Brazil), the Eastern Brazilian Pegmatite Province and related mineral resources. Geological Society, London, Special Publications, 350(1), 25-51.

Penman, D. E., & Rooney, A. D. (2019). Coupled carbon and silica cycle perturbations during the Marinoan snowball Earth deglaciation. Geology, 47(4), 317-320.

Pierrehumbert, R. T. (2004). High levels of atmospheric carbon dioxide necessary for the termination of global glaciation. Nature, 429(6992), 646-649.

Preiss, W. V. (1987). The Adelaide Geosyncline: Late Proterozoic stratigraphy, sedimentation, palaeontology and tectonics (Vol. 53): Department of Mines and Energy.

Preiss, W. V., Gostin, V. A., McKirdy, D. M., Ashley, P. M., Williams, G. E., & Schmidt, P. W. (2011). The glacial succession of Sturtian age in South Australia: the Yudnamutana Subgroup. Geological Society, London, Memoirs, 36(1), 701-712.

Preiss, W. V., Drexel, J. F., & Reid, A. J. (2009). Definition and age of the Kooringa Member of the Skillogalee Dolomite: host for Neoproterozoic (c. 790 Ma) porphyry related copper mineralisation at Burra. MESA Journal, 55, 19-33.

Rao, C. P., Goodwin, I. D., & Gibson, J. A. E. (1998). Shelf, coastal and subglacial polar carbonates, East Antarctica. Carbonates and Evaporites, 13(2), 174-188.

Rooney, A. D., Strauss, J. V., Brandon, A. D., & Macdonald, F. A. (2015). A Cryogenian chronology: Two long-lasting synchronous Neoproterozoic glaciations. Geology, 43(5), 459-462.

Schrag, D. P., Higgins, J. A., Macdonald, F. A., & Johnston, D. T. (2013). Authigenic carbonate and the history of the global carbon cycle. Science, 339(6119), 540-543.

Shuster, A. M., Wallace, M. W., Hood, A.v.S., & Jiang, G. (2018). The Tonian Beck Spring Dolomite: Marine dolomitization in a shallow, anoxic sea. Sedimentary Geology, 368, 83-104.

Spence, G. H., Le Heron, D. P., & Fairchild, I. J. (2016). Sedimentological perspectives on climatic, atmospheric and environmental change in the Neoproterozoic Era. Sedimentology, 63(2), 253-306.

Spencer, A.M. (1971). Late pre-Cambrian glaciation in Scotland (No. 6). Blackwell Science Incorporated.

Stroncik, N. A., & Schmincke, H. U. (2001). Evolution of palagonite: Crystallization, chemical changes, and element budget. Geochemistry, Geophysics, Geosystems, 2(7).

This article is protected by copyright. All rights reserved

Author Manuscript

977 Tucker, M. E. (1982). Precambrian dolomites: petrographic and isotopic evidence that they
978 differ from Phanerozoic dolomites. Geology, 10(1), 7-12.
979 Walker, J. C. G., Hays, P. B., & Kasting, J. F. (1981). A negative feedback mechanism for
980 the long-term stabilization of Earth's surface temperature. Journal of Geophysical
981 Research: Oceans, 86(C10), 9776-9782.
982 Wallace, M. W., Hood, A.v.S., Fayle, J., Hordern, E. S., & O'Hare, T. F. (2019).
983 Neoproterozoic marine dolomite hardgrounds and their relationship to cap dolomites.
984 Precambrian Research, 328, 269-286.
985 Walter, M., Veevers, J., Calver, C., Gorjan, P., & Hill, A. (2000). Dating the 840–544 Ma
986 Neoproterozoic interval by isotopes of strontium, carbon, and sulfur in seawater, and
987 some interpretative models. Precambrian Research, 100(1-3), 371-433.
988 Young, G. M., & Gostin, V. A. (1991). Late Proterozoic (Sturtian) succession of the North
989 Flinders Basin, South Australia: an example of temperate glaciation in an active rift
990 setting (Vol. 261). Boulder, USA: Geological Society of America Special Paper.
991 Yu, W., Algeo, T. J., Du, Y., Zhou, Q., Wang, P., Xu, Y., . . . Pan, W. (2017). Newly
992 discovered Sturtian cap carbonate in the Nanhua Basin, South China. Precambrian
993 Research, 293, 112-130.
994 Zeebe, R. E., & Tyrrell, T. (2019). History of carbonate ion concentration over the last 100
995 million years II: Revised calculations and new data. Geochimica et Cosmochimica
996 Acta, 257, 373-392.
997 Zhang, Q.-R., Chu, X.-L., & Feng, L.-J. (2011). Neoproterozoic glacial records in the
998 Yangtze Region, China. Geological Society, London, Memoirs, 36(1), 357-366.
999 Zhou, Q., Du, Y., Yan, J., Zhang, M., & Yin, S. (2007). Geological and geochemical
1000 characteristics of the cold seep carbonates in the Early Nanhua System in Datangpo,
1001 Songtao, Guizhou Province. Earth Science–Journal of China University of
1002 Geosciences, 32, 845-852.
1003
1004 **Figure captions**
1005 **Figure 1**. a) Sturtian glacial stratigraphy of the Flinders Ranges and surrounding units
1006 (modified from Preiss et al., 2011). b) Location of the Holowilena South (Fig. 2) and
1007 Oraparinna (Fig. 3) field areas, South Australia.
1008 **Figure 2.** Stratigraphic sections and geological map of Holowilena South (modified after
1009 Lechte and Wallace, 2015). Scale applies to all sections. Note the presence of dolomite and
1010 dolomitic siltstone throughout the glacial sequence.

This article is protected by copyright. All rights reserved

Author Manuscript

Figure 3. Oraparinna stratigraphic section (modified from Lechte et al., 2019) with locality map. Note the presence of dolomite and dolomitic siltstone.

Figure 4. Field photographs from Holowilena South (a)-(g) and Oraparinna (h)-(i) showing dolomitic lithologies of the Sturtian glacial succession. a) Laminated dolomite of the Warcowie Dolomite Member. b) Wilyerpa Formation, interbedded dolomite (D) and dolomitic shale. c) Dolomite beds (D) in the Wilyerpa Formation, showing deformation by granite dropstone (arrow). d) Dolomitic siltstone beds (yellow/brown) within green siltstones showing grading and soft sediment deformation (arrow), Wilyerpa Fm. e) Dolomite and dolomitic siltstones (yellow), with sand lenses, gravels and outsized clasts, Wilyerpa Fm. f) Dolomitic matrix in diamictite, Wilyerpa Fm. g) Distinctive intraclastic carbonate clast likely derived from the Tonian Skillogalee Dolomite in a dolomitic diamictite from the lower Wilyerpa Fm. h) Dolomitic siltstones with dropstones, Wilyerpa Formation, Oraparinna. i) Dolomitic siltstones (D) interbedded with ferruginous shales (red) of the upper Holowilena Ironstone (hammer for scale).

Figure 5. Thin section photomicrographs of syn-glacial carbonates, which occur in a range of facies at Holowilena South. See Lechte et al. (2019) for more detail on facies interpretations. a)-c) Thin section images of increasing magnification of a laminated dolomite bed in the Holowilena Ironstone. Sample HO2-22.5. Finely laminated, rhythmic dolomicrite–dark in (a) and highly birefringent in b)-c)–is interlaminated with quartz sand layers with irregular thicknesses and erosive bases (arrow). Quartz layers may represent pulses of sedimentation from meltwater discharge in ice-proximal settings. d) Ice-distal turbidites of quartz (showing sediment loading) and interlaminated dolomicrite, Wilyerpa Fm., Sample HCS-148A. e)-f) Wilyerpa Fm., sample HCS-136.5 from dolomite bed within dolomitic siltstone facies in increasing magnification. Dolomicrite- dark in e), highly birefringent in f)– is interlaminated by quartz and detrital mineral layers with erosive bases (arrow) as evidence of syn-sedimentary reworking of dolomite. g)-i) Sample H-W from a dolomite bed with sand and gravel layers in the lower Wilyerpa Fm., from outcrop documented in Fig. 4e. Rounded clasts are of many different lithologies and are interbedded with dolomite–at the base of g)-h)–and dolomitic siltstone–top of (h). At high magnification (i), highly birefringent dolomite crystals are euhedral to anhedral. Sample interpreted as reworked glacial sediment in intermittent mass flows deposited into ice-proximal to ice-distal dolomicrite-dolomite silt beds. j)-k) Ice-contact diamictite facies of the Pualco Tillite, showing a range of clast types (j) with a finely crystalline dolomite and quartz silt matrix (k) Sample Pualco-1. l) Diamictite facies of the

This article is protected by copyright. All rights reserved

Author Manuscript

Wilyerpa Fm. with finely-crystalline dolomite matrix (high birefringent) and quartz grains. Sample HCS-202.

Figure 6. Cathodoluminescence photomicrographs (a)-(b) and BSE photomicrographs (c)-(e) of the Warcowie Dolomite Mb., Holowilena South. a) and b) Bright-dull red luminescence of dolomite matrix (non-luminescent phases are quartz, blue luminescent phases are feldspars and green luminescent phases are apatite). The stratigraphically higher sample, (b), has relatively more dolomite than (a), represented by an increased amount of bright-dull-red luminescent dolomite and less non-luminescent quartz, and shown as increased carbonate content in Table S1 (35-36% carbonate at the base and ~58-65% at the top of the bed). c)-e) BSE photomicrographs of euhedral dolomite crystals (D) growing within sediments composed of detrital K-feldspar (K), mica (M) and quartz (Q). Note compositional zoning in dolomite crystals (arrow). Brightness difference appears to be from variations in iron concentrations. Using semi-quantitative EDS, bright areas have up to 5 mass percent Fe, whereas darker parts of the crystal have iron concentrations commonly below detection.

Figure 7. BSE photomicrographs of matrix dolomite crystals in syn-glacial sediments from Holowilena South. a) Euhedral to anhedral dolomite crystals with inner dark cores and lighter outer Fe-rich rims. Laminated dolomite facies, Wilyerpa Fm., sample HCS-148A. b) Zoned dolomite crystals (D) growing within sediments composed largely of detrital mica (M) and quartz (Q), Holowilena Ironstone dolomite bed, sample HO2-22.5. c) Zoned dolomite crystals (D) intergrowing between detrital minerals including quartz (Q). Bright mineral is hematite. Sample taken from diamictite facies of the basal Wilyerpa Fm. d) Euhedral, complex-zoned dolomite crystals growing with quartz (Q). Bright mineral is hematite. Sample from dolomite bed within dolomitic siltstones, Wilyerpa Fm., HCS-136.5.

Figure 8. Cross plot of carbonate carbon and oxygen isotope data, showing distinct isotopic differences between Sturtian glacial dolomites (warm colours: Oraparinna and Holowilena South, this study; Appila Tillite, Crossing and Gostin, 1994; Wilyerpa Fm., McKirdy et al., 2001), underlying Burra Group carbonates (grey: Crossing and Gostin, 1994; Hill and Walter, 2000; Frank and Fielding 2003) and detrital dolomite clasts in Sturtian diamictites (blue: Appila Tillite, Crossing and Gostin, 1994).

Figure 9. Variability in model outputs of syn-glacial carbonate burial, seawater Mg/Ca and glacial duration (blue shading) under different PreCOSCIOUS modelling scenarios. Note change of scale across experiments in carbonate burial and silicate weathering flux. a) Standard PreCOSCIOUS model with higher deglaciation threshold. Carbonate burial drops to

This article is protected by copyright. All rights reserved

Author Manuscript

zero during glaciation but is extensive following deglaciation. Magnesium declines to very low concentrations. b) "Constant flux" and c) "limited weathering feedback" model outputs to fit ~50 My Sturtian by invoking some chemical weathering during glaciation (see main text for model details). Note limited carbonate burial during glaciation (up to ~1.6×10^{13} Mol/yr) and less extensive cap carbonate precipitation after glaciation. Seawater magnesium concentrations are relatively stable through glaciation. 'Ω' refers to calcite saturation state, though sensitivity tests which consider the solubilities of dolomite and magnesite can be found in the Supplementary Information.

Author Manuscript

This article is protected by copyright. All rights reserved

gbi_12470_f1.pdf

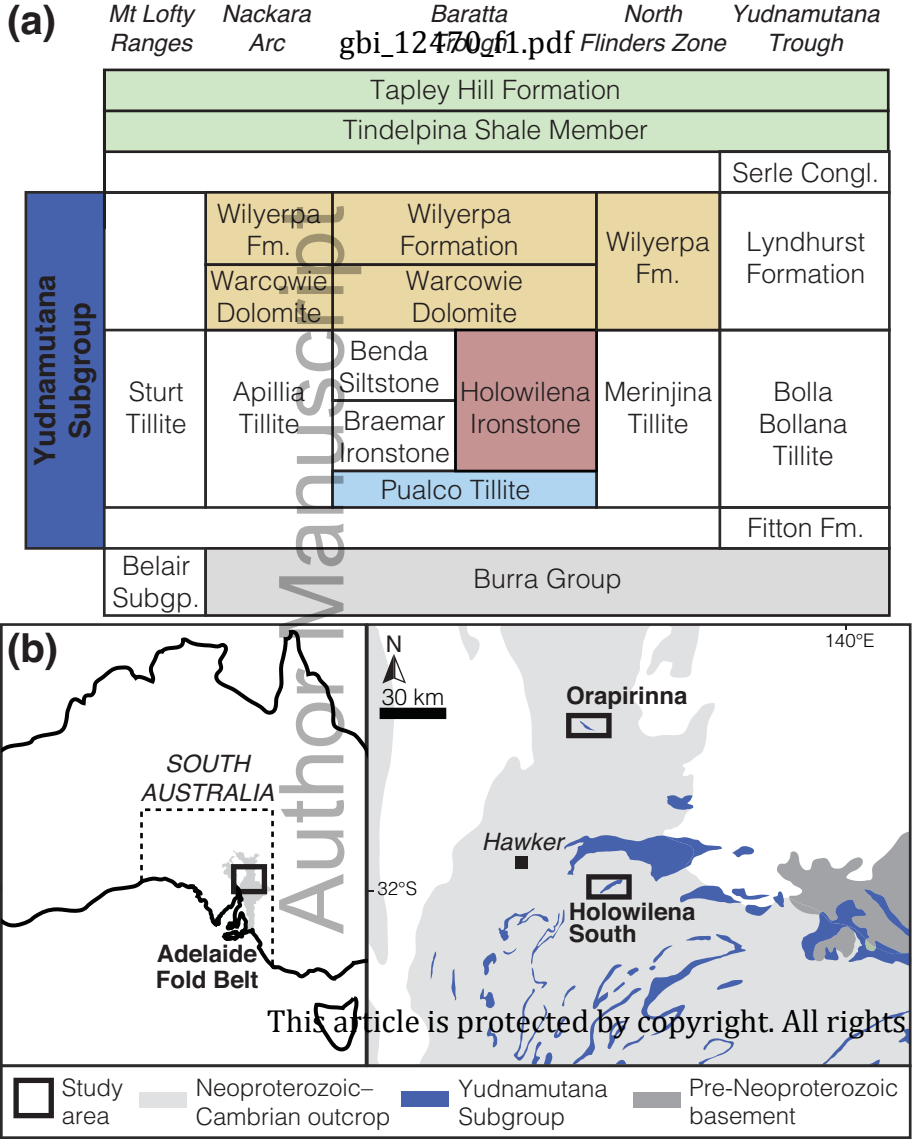

Author Manuscript

This article is protected by copyright. All rights

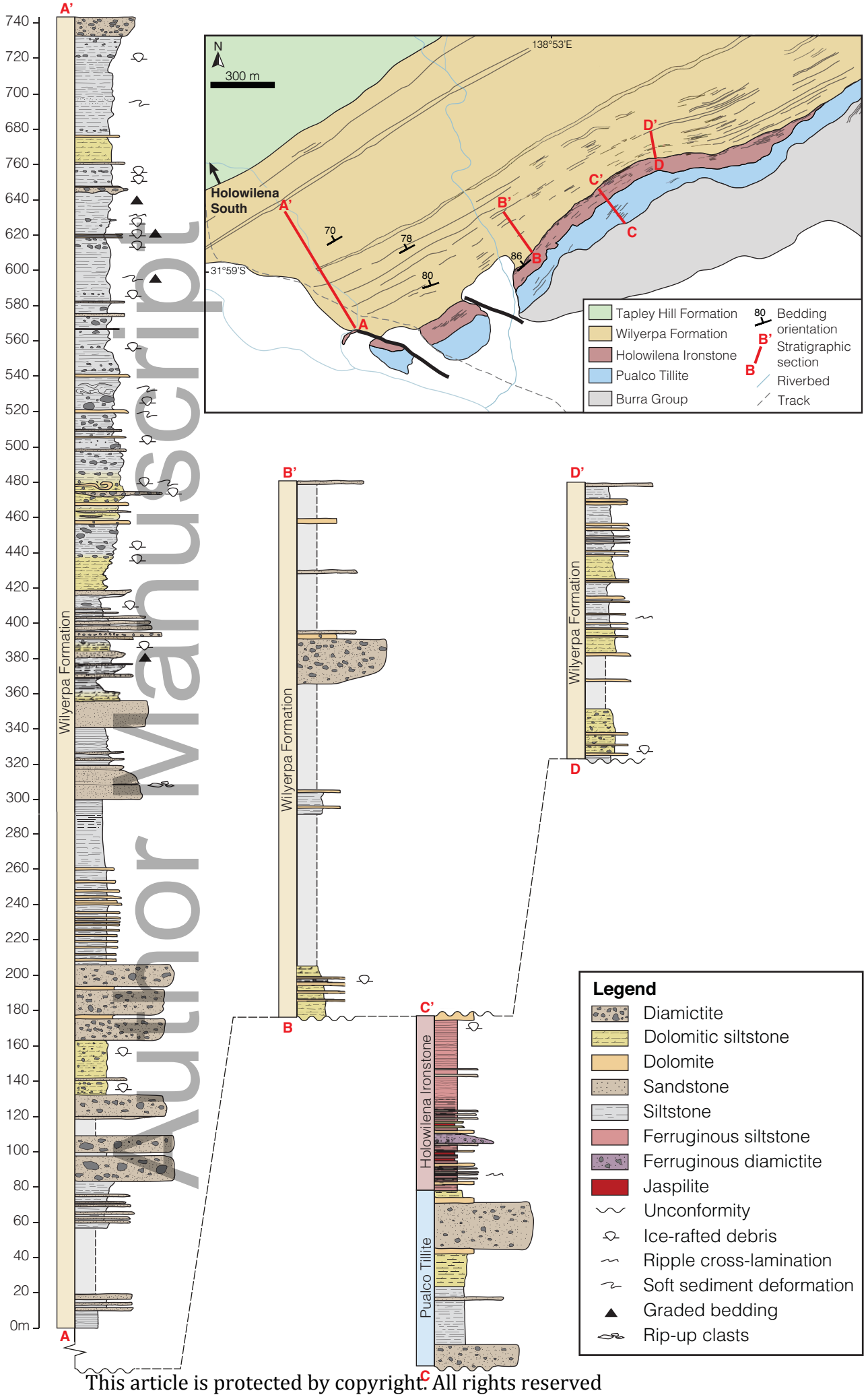

Author Manuscript

This article is protected by copyright. All rights reserved

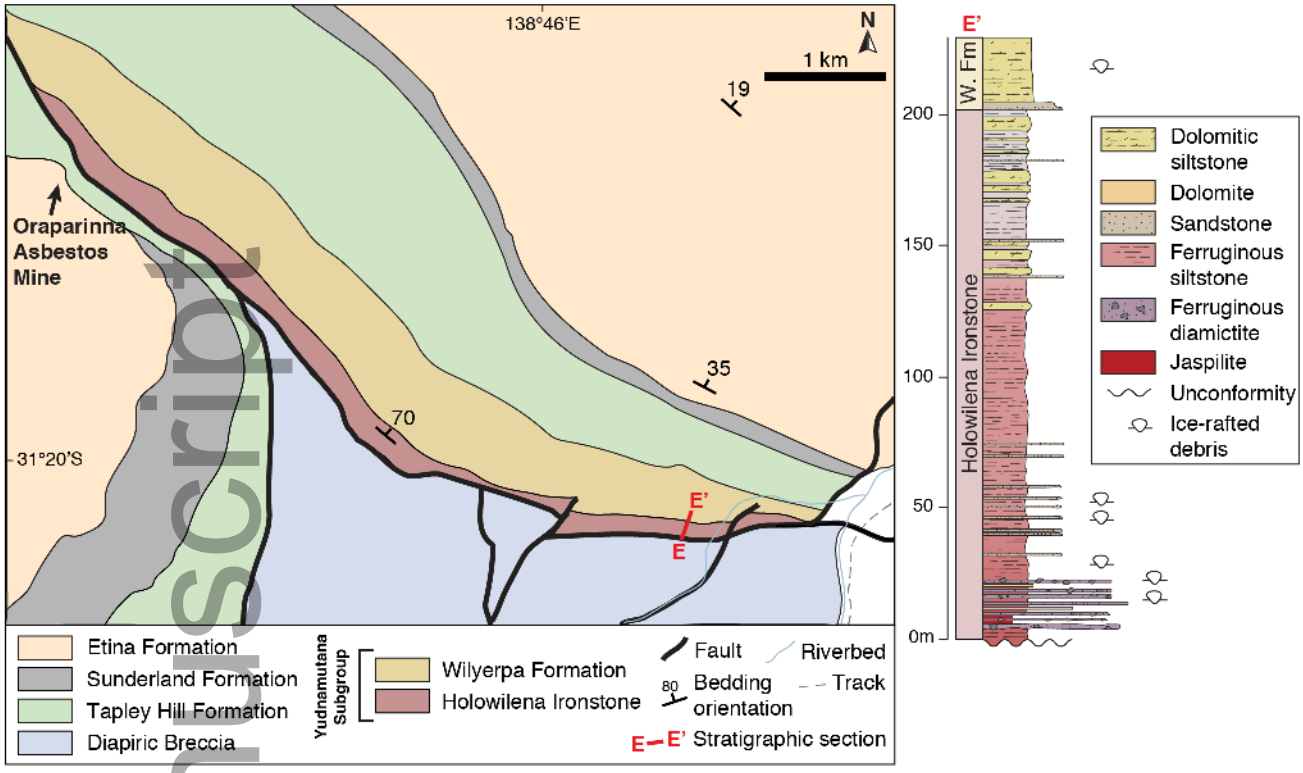

gbi_12470_f3.png

Author Manuscript

This article is protected by copyright. All rights reserved

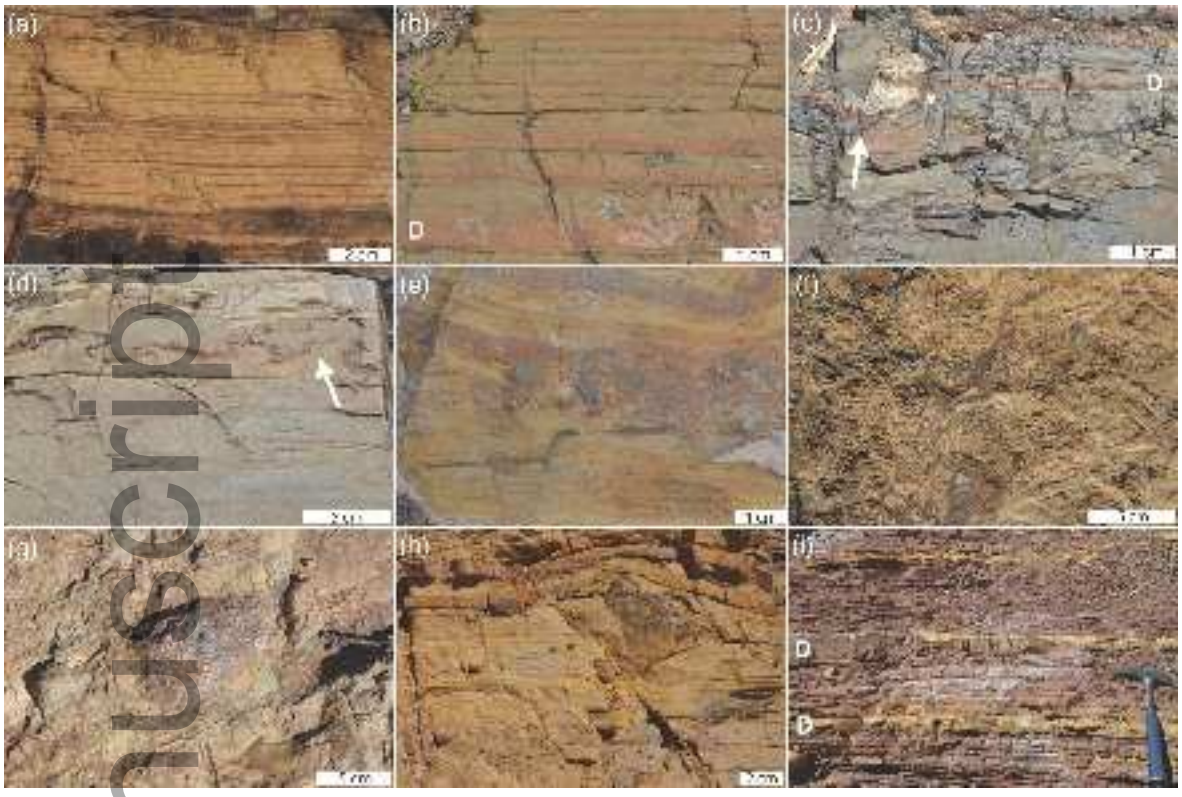

gbi_12470_f4.tif

Author Manuscript

This article is protected by copyright. All rights reserved

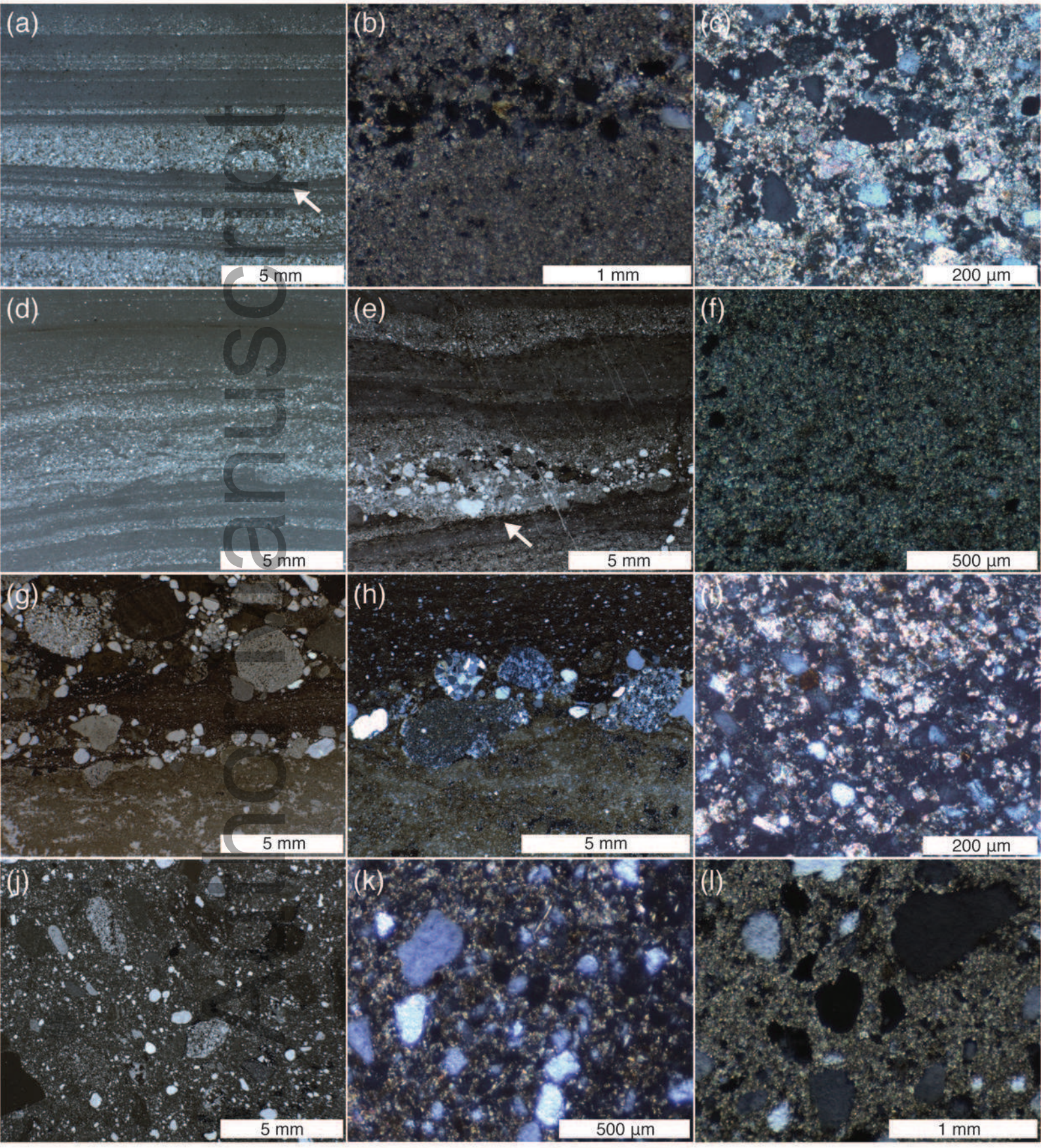

This article is protected by copyright. All rights reserved

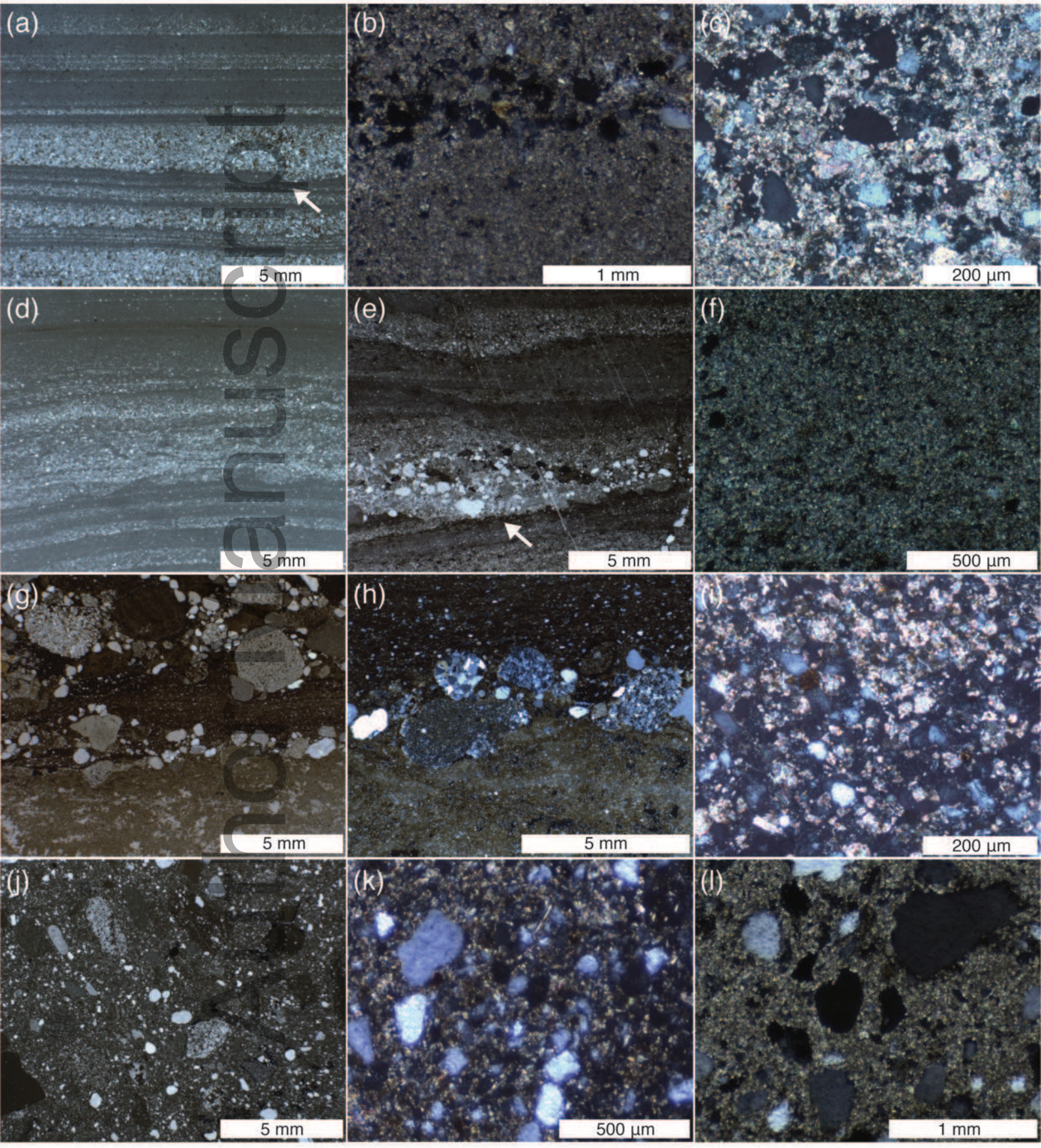

This article is protected by copyright. All rights reserved

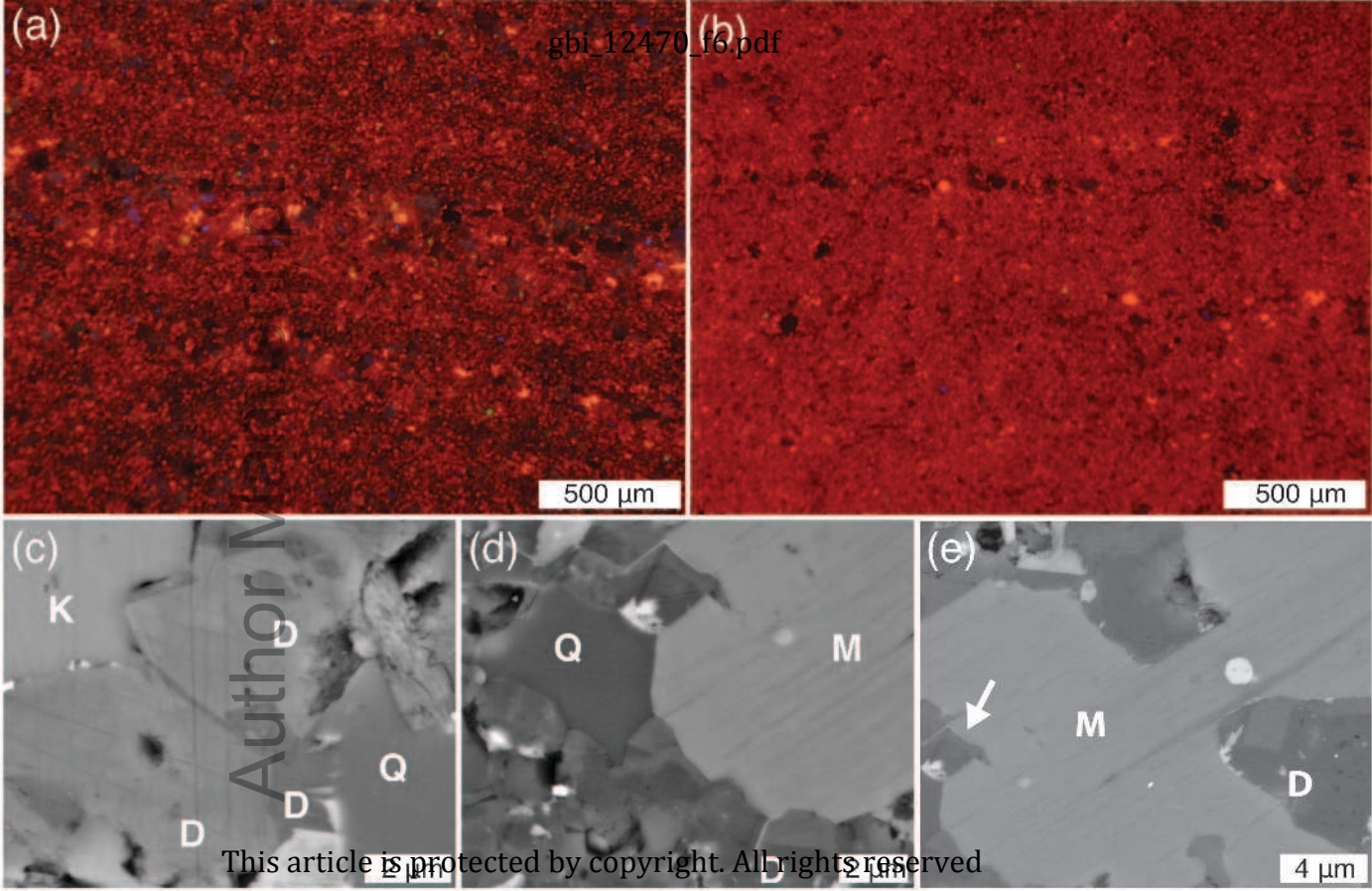

This article is protected by copyright. All rights reserved

gbi_12470_f7.pdf

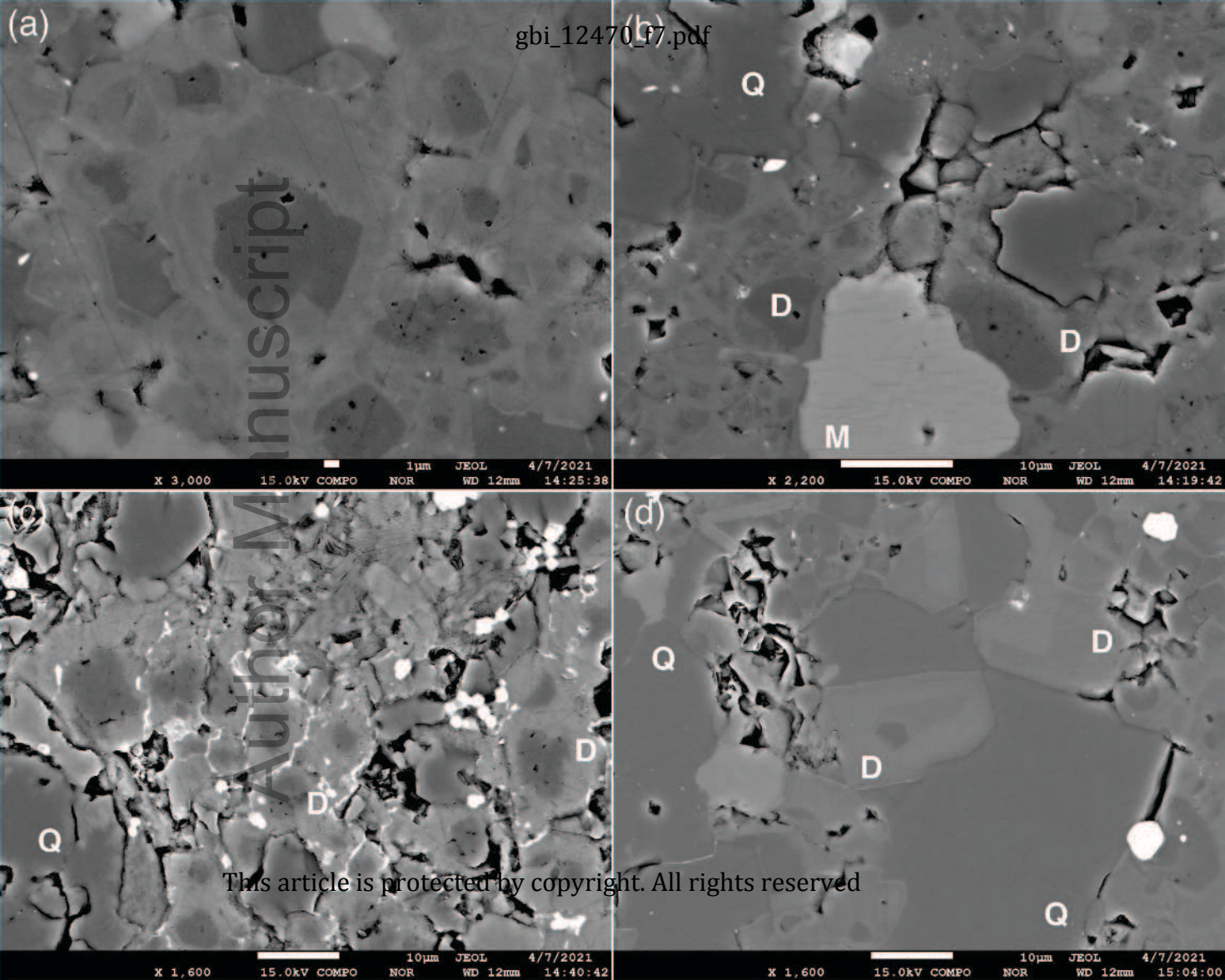

Author Manuscript

This article is protected by copyright. All rights reserved

gbi_12470_f8.pdf

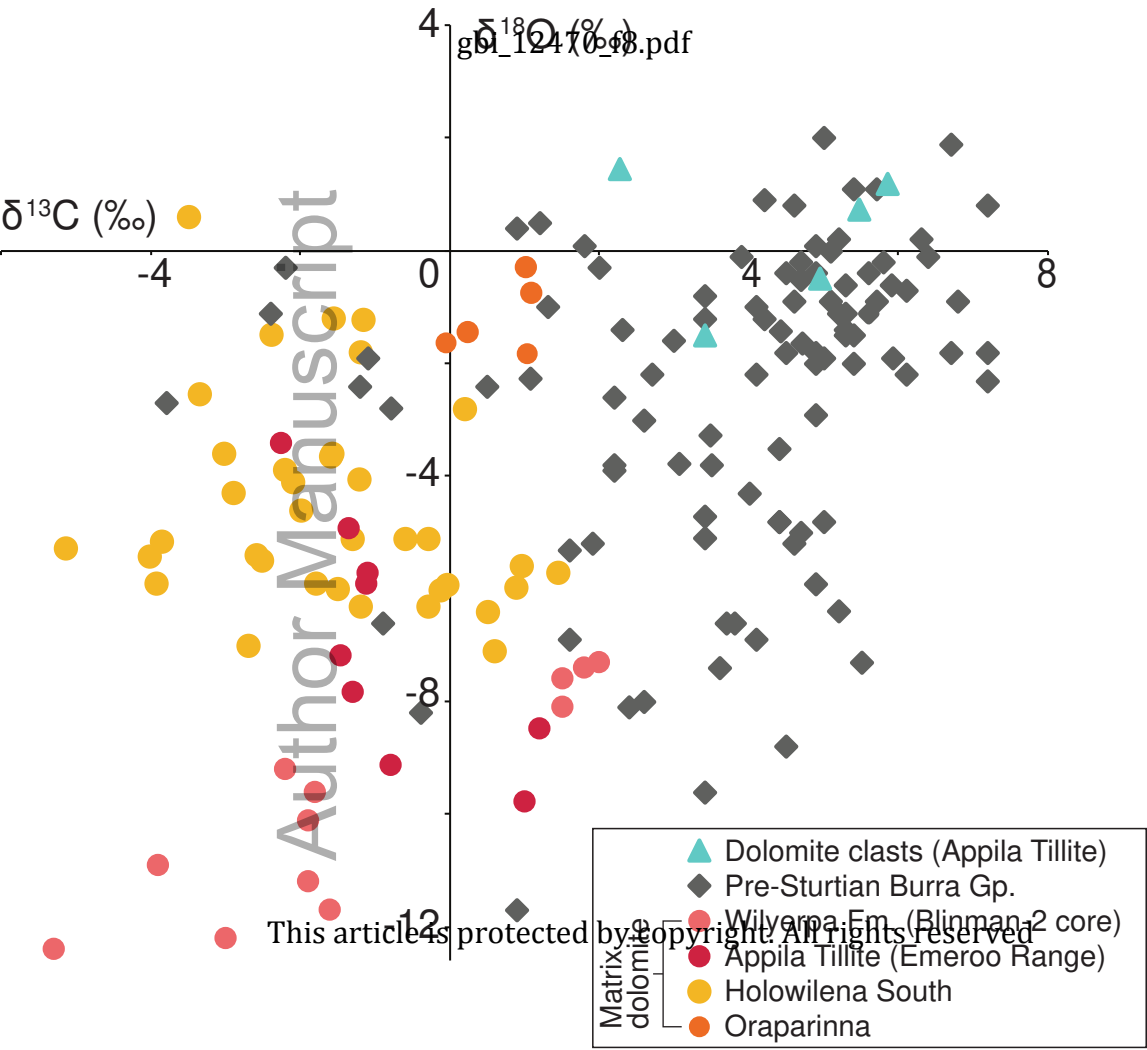

Author Manuscript

This article is protected by copyright. All rights reserved

gbi_12470_f9.pdf

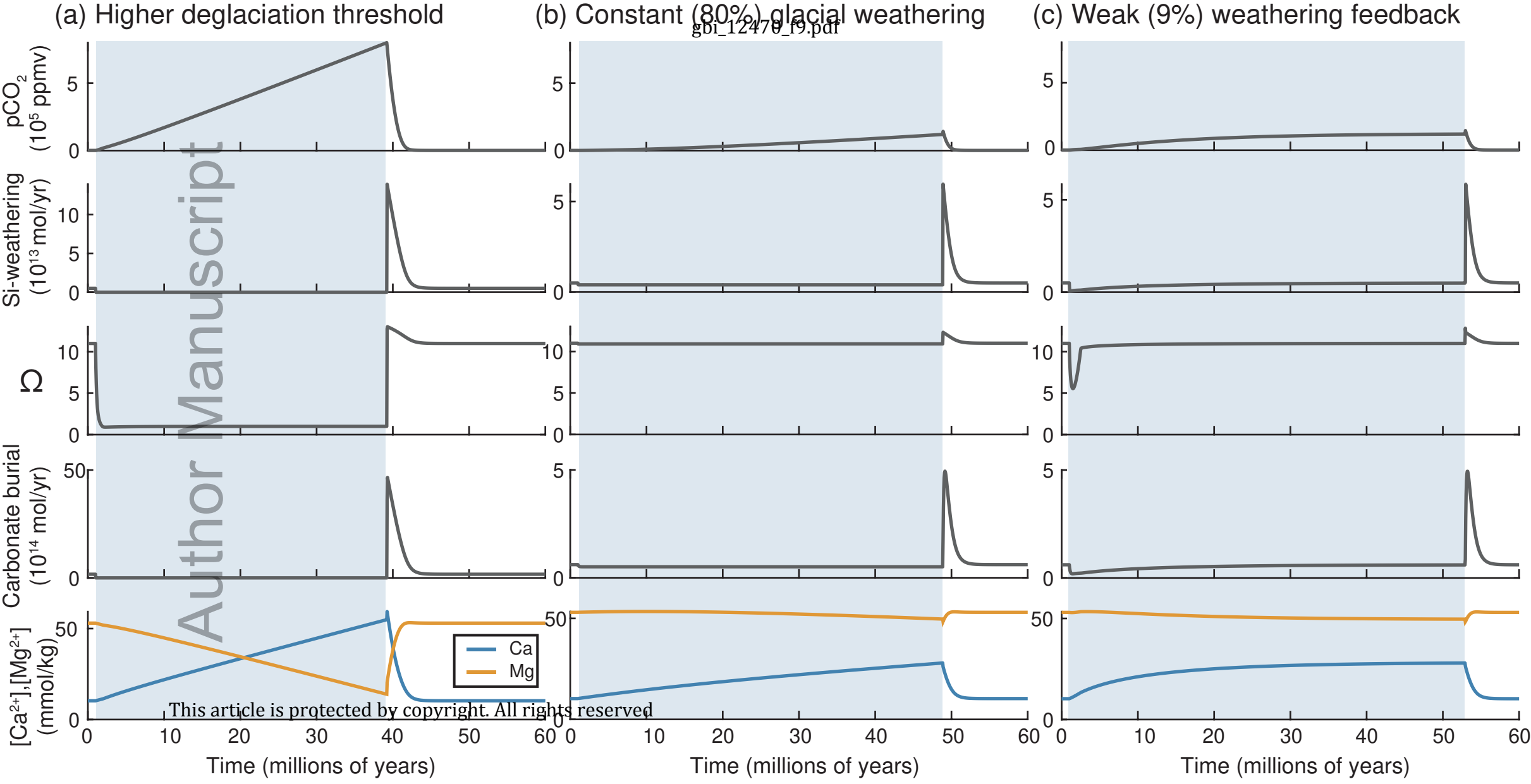

Author Manuscript

This article is protected by copyright. All rights reserved